

https://dspace.org/

Modeling of the corona ionization space propulsion system

Pokaha, Marius Tchonang

2011-10-07
http://hdl.handle.net/10539/10493

Downloaded from a DSpace repository. https://dspace.org/

M O D E L I N G O F T H E C O R O N A I O N I Z A T I O N S P A C E P R O P U L S I O N S Y S T E M

Marius Tchonang Pokaha

July 2011

A dissertation submitted to the faculty of Science, university of the Witwatersrand, Johannesburg, in fulfillment of the requirements for the degree of Master of Science.

Acknowledgement

The author would like to thank a number of people who provided help and support throughout the project:

My supervisor, Dr. Phil. Ferrer, School of Physics, University of the Witwatersrand, for his dedication to my supervision, which went far beyond his duty.

All my friends for their emotional support and for their help in proofreading the final report.

Prof. J. Rodrigues, head of the School of Physics, University of the Witwatersrand and the National Institute of Theoretical Physics (NITheP) for the financial support they provided throughout the project.

Declaration

I declare that this dissertation is my own, unaided work. It is being submitted for the degree of Master of Science in the University of the Witwatersrand, Johannesburg. It has not been submitted before for any degree or examination in any other University.

……

Marius P. Tchonang

…… Day of …… 2011

Abstract

In this thesis, a novel type of electrostatic thruster is introduced. The Corona Ionization (CorIon) Space Propulsion system is an electrostatic propulsion system intended for use on satellites and for deep space probes. It makes use of the corona ionization mechanism to create the needed propellant ions. This same mechanism is also responsible for the thrust, thereby reducing its size and complexity.

First, the effects of incomplete ionization of propellant molecules is discussed and conclusions drawn.

Next, a mathematical model describing the electric field characteristics is derived. Considering the needle tip as a point charge and the exhaust plume to be cylindrically symmetric with a constant spread angle, the resultant electric field of both the needle tip and the produced ions obeys Poisson's equation. The charge density is obtained from the relationship between the drift velocity and the current. In order to solve the differential equation, we consider the electric field to only change in the radial direction so that Poisson's Equation is reduced to its radial part. This differential equation is solved to yield the electric field of the system. Some results are discussed. By integrating the electric field the relationship between the potential difference and the current of propellant ions is obtained. This relationship also yields insight into the ionization efficiency.

Following this, an expression for the thrust is derived via two different methods: The first uses the energy conservation, and is termed "Vector heating". The ions are viewed as a current heating the neutrals in the plume in the direction away from the needle. A temperature can be derived for the plume, and the resulting average gas velocity estimated from molecular theory. Finally, using the rocket thrust equation, an expression for the thrust is obtained.

The second, more conventional method uses electrostatic repulsion to calculate the recoil on the needle: from the electric field computed for the system, an expression for the Coulomb forces on the ionized propellant can be derived. The recoil on the needle will experience the same force, resulting in thrust.

Finally, the theoretical predictions for the various parameters are compared to experimental data. From this comparison, it is seen that there is a reasonable agreement between the experimental data and the model even though the electrostatic prediction underestimates the thrust of the system.

Table of Contents

Acknowledgement i

Abstract iii

List of Figures viii

List of Tables xi

List of Symbols xii

Chapter 1 1

Introduction 1

1.1 Motivation and identification of opportunity 2

1.2 Statement of objectives 3

Chapter 2 4

Existing technologies 4

2.1 Definitions and fundamentals 4

2.2 Existing systems 8

2.2.1 Thermodynamic systems 9

2.2.1 Electrodynamics systems 13

2.2.1.2 Electromagnetic thrusters 14

2.2.1.3 Ion Engine 17

Chapter 3 23

Corona Discharge and the Proposed Concept 23

3.1 Corona Discharge 23

3.1.1 Some properties of Plasma 23

3.1.2 Ionization mechanism 24

3.1.3 Field intensified and corona ionization 25

3.2 Proposed Concept 29

3.3 Basic requirement of the system 30

3.3.1 The Needle 30

3.3.2 The propellant 32

3.4 Effect of the incomplete ionization of the propellant 33

Chapter 4 40
Electric field and Potential as Function of the Current 40
4.1 Exhaust plume description 41
4.2 Relationship between the current and the voltage 43
4.2.1 Electric field of the system 44
4.2.2 Relationship between the current and voltage 53
Chapter 5 57
Derivation of the Thrust 57
5.1 Vector heating 57
5.2 The Electrostatic method 60
Chapter 6 64
Prior Experimental Results 64
6.1 Experimental objectives 64
6.2 Experimental equipment and setup 64
6.3 Experiment 1 67
6.3.1 Experiment 67
6.3.2 Presentation of results 68
6.4.2 Presentation of results 70
Chapter 7 72
Comparison of Theory and Experiment 72
7.1 Voltage Vs Current comparison 74
7.2 Power Vs Current comparison 74
7.3 Thrust comparison 75
7.4 Further comparison: Effects of the mass flow rate 77
Chapter 8 79
Conclusion and Outlook 79
8.1 Conclusion 79
8.2 Outlook 80
Appendix A 82
Number density 82

Appendix B 85
Calculation of the Electric Field 85
Appendix C 87
Table of Data of the graphs in Chapter 7 87
References 89

List of Figures

Figure 2.1: a typical solid rocket motor...……9

Figure 2.2: a typical liquid propellant rocket motor...…….....10

Figure 2.3: schematic of a two-stage rocket...…….....11

Figure 2.4: some famous European launchers...……....11

Figure 2.5: concept of the NERVA engine reactor……...……12

Figure 2.6: 1 kW hydrogen arc jet plume...…….....13

Figure 2.7: schematic of a magnetoplasmadynamic thruster…….15

Figure 2.8: schematic of a Hall Effect thruster……..16

Figure 2.9: schematic of an ablative pulsed plasma thruster...……...17

Figure 2.10: ion thruster schematic……18

Figure 2.11: electrostatic ion engine operation……..19

Figure 2.12: close up-view of the NSTAR ion engine...…….....20

Figure 2.13: Deep Space I spacecraft during testing…….21

Figure 3.1: schematic of a typical gaseous discharge circuit…….26

Figure 3.2: current-voltage relationship for a gas discharge process...…….27

Figure 3.3: ionization efficiency graph…….....28

Figure 3.4: schematic of the plume exiting the positively charged needle……29

Figure 3.5: Corona onset voltage variation with electrode radius ……32

Figure 3.6: Ionization energy of different noble gases …….33

Figure 3.7: comparison of the two tubes (complete and incomplete ionization)…..34

Figure 3.8: schematic of a cross sectional volume...…….34

Figure 4.1: schematic of the exhaust plume...……...41

Figure 4.2: model of the plume in spherical coordinates…….....43

Figure 4.3: model of the point charge inside a sphere…….....46

Figure 4.4: outward flux of neutral gas molecules……48

Figure 4.5: Electric field as a function of the distance from the needle tip for some values of the current……53

Figure 4.6: voltage as a function of the current…….55

Figure 4.7: power as a function of the current...……56

Figure 4.8: resistance as a function of the current……....56

Figure 5.1: Molecules escaping a box at approximately thermal velocity……58

Figure 5.2: effect of the electrical energy on the average velocity……....58

Figure 5.3: model of the plume for the thrust……....60

Figure 6.1: final sensor and thruster setup..……...65

Figure 6.2: Equipment layout...……66

Figure 6.3: Vacuum chamber and equipment...…….67

Figure 6.4: Measurements of current for experiment 1...……..68

Figure 6.5: Electrical power usage for experiment 1...…….....69

Figure 6.6: Measurements of thrust for experiment 1...……69

Figure 6.7: Measurements of current for experiment 2**...**…….**.....**70

Figure 6.8: Electrical power usage for experiment 2**...**……..70

Figure 6.9: Measurements of thrust for experiment 2**...**……71

Figure 6.10: plume of the CorIon thruster in operation……71

Figure 7.1: comparison of theoretical and experimental voltage…….**.....**74

Figure 7.2: comparison of theoretical and experimental power**...**…….75

Figure 7.3: comparison of theoretical and experimental thrust**.....**……..76

Figure 7.4: change of the potential difference with the flow rate……..78

Figure A.1: Schematic of a gas exiting a tube of radius d…….83

List of Tables

Table 3.1: Variation of the electric field with the electrode diameter for some materials……..31

Table 7.1: estimation of experimental data (onset voltage$= 1250\ V$) ...……....72

Table 7.2: physical dimensions of the thruster……..73

Table 7.3: gas properties……73

Table 7.4: theoretical performance of the thruster……73

Table 7.5: change in voltage at different flow rate at the same current…….77

Table A.1: calculated parameters of the thruster……...87

List of Symbols

- F: thrust produced by the rocket
- $\dot{m}$: propellant mass flow rate
- V_e: exhaust velocity
- V: final vehicle velocity
- m_0 : initial vehicle mass
- m_f : final vehicle velocity
- I_t: total impulse
- I_s: specific impulse
- m_p : total propellant mass
- g_0 : acceleration due to gravity at sea level
- MR : vehicle mass ratio
- W_0 initial weight
- P_{jet} : power carried by the ejected matter
- P_0 : input power
- η_T : thruster efficiency
- α : specific power
- θ_m : spread angle of the plume
- E_{ion} : energy cost per ion
- M_{out}^{+} : ion mass flow
- M_{int} : mass flow of propellant into the ion source
- σ : scattering cross section
- V_0 : Corona onset potential
- M : molecular mass
- n : number density of neutrals

- λ : ion mean free path
- K_B : Boltzmann constant

Chapter 1

Introduction

The chemical rocket has performed well in launching military and commercial satellites from earth into orbit, and remains the only viable technology to do this [1, 2, 3]. But for deep space probes, orbit raising and station keeping, chemical rockets may not be the best choice [1]. Researchers look to different, more adequate or efficient propulsion technologies, such as, amongst others electric propulsion, nuclear propulsion and cold gas thrusters.

Much research has been done in the field of electric propulsion from the first laboratory test in 1960 to the first successful flight on the NASA's electric propulsion system Deep Space I in 1998 [4]. In essence, chemical rockets transport things from earth to orbit and more efficient systems are used after. Electric propulsion for generation of thrust in outer space is an active field of research, where many system designs are under investigation [2, 5]. Electric propulsion has been identified as being amongst the most efficient propulsion systems, in terms of the terminal velocity the system can reach after consumption of all fuel [3, 6]. This efficiency is mainly due to the very high exit velocities of the propellant which can be reached by electromagnetic systems, as well as their overall good performance regarding propellant utilization [3, 6, 7]. However, electric propulsion suffers from some problems that can significantly affect the performance and the lifetime of the spacecraft they are used on. The closest related system that can be used for comparison is the ion engine, which has distinguished itself through efficiency and

has shown to be fairly reliable on actual space missions (See section 2-2 for more details).

1.1 Motivation and identification of opportunity

There are many factors influencing the design of an electric propulsion system, such as efficiency, reliability, durability, mass, etc. Current electric propulsion systems have some components that can reduce the lifetime of the system. For example collision of heavy ions with the acceleration grid causes erosion that leads to the reduction of the system performances and can even cause its failure [1, 8].

Another problem of electric propulsion is the energy cost for the production of an electron/ion pair. Because ionization takes place in an ionization chamber, there is recombination resulting to a waste of energy, reducing the efficiency of the system. The actual ionization energy of an atom varies between 10 and 15 eV but testing has shown an energy cost of some 15 times this energy [9, 10]. The need of an ionization chamber also increases the size and the mass of the system, reducing the payload.

These issues can be addressed if one can develop an electric propulsion system that does not use a physical acceleration grid or if a more efficient ionization mechanism can be used.

Dr Phil Ferrer and Mr T. Lafleur developed a thruster based on the use of corona ionization which is amongst the most efficient ionization mechanisms for certain processes [11, 12]. They did a series of proof-of-concept tests. And these tests showed the viability of their proposal and so opened doors to more research in order to improve their results.

1.2 Statement of objectives

Investigation of the design of an electric propulsion system involves techniques where the designs are tested via theory, computational simulations and tests in a space-like environment. In chapter 2, an overview of the existing technology with their advantages and disadvantages is given. Then, after discussing different ionization mechanisms and the corona in chapter 3, we then use the physical parameters of the system to develop its first mathematical model. This model is used to predict the electric field of the system and the relationship between the voltage and the current in chapter 4. Chapter 5 uses again the mathematical model to predict the thrust produced by the thruster. Chapter 6 presents prior experimental results that we use to test the validity of our model in the last chapter, and from there conclusions will be drawn and recommendations made for further research.

Chapter 2

Existing technologies

2.1 Definitions and fundamentals

A rocket is a device which propels itself by emitting a jet of matter. The momentum carried away by the jet results in a force acting so as to accelerate the rocket in the direction opposite to that of the jet. So the velocity and the mass of the rocket change with time [1, 2, 8]. Rocket science is not a fundamental subject and its basic principles are those of mechanics, electrodynamics, thermodynamics and chemistry.

Propulsion is achieved by applying a force to a vehicle. That is, accelerating the vehicle or by maintaining a given velocity against a resisting force. The Russian Konstantin Tsiolkovsky, based on the fact that the rocket mass decreases, and by Newton's third law, gave the accelerating force (which is the thrust) as a function of the mass flow rate and the exhaust velocity of the jet as follows [1, 2, 8]

$$F = \dot{m} V_e \ , \tag{2.1}$$

Where F is the thrust or the accelerating force, $\dot{m}$ the mass flow rate or the change in mass of the rocket and V_e the exhaust velocity or the velocity of the ejected jet relative to the rocket.

By solving the Tsiolkovsky rocket equation, one obtains the vehicle velocity [1, 2, 3]:

$$V = V_e \ln \frac{m_0}{m_f} \ . \tag{2.2}$$

Here, m_0 is the mass of the rocket at ignition, and m_f is the final mass of the rocket. This formula is the basis of all rocket propulsion. We will focus now on electric propulsion technology, as the device studied in this project belongs to that category of rocket. Beside the thrust, another important parameter of propulsion systems is the Total Impulse I_t which is the integral of the thrust force F over the burning time t,

$$I_t = \int_0^t F dt \ . \tag{2.3}$$

If F is constant,

$$I_t = F.t \ . \tag{2.4}$$

The total impulse measures the total amount of momentum imparted to the rocket by the motor, and determines how high the motor can propel the rocket against gravity [1, 2, 3]. In giving performance characteristics of a propulsion system, many authors use the specific impulse instead of the total impulse. The specific impulse I_s is the total impulse per unit weight of propellant; it defines how long the propellant can accelerate its initial mass. The larger I_s, the better the performance of the engine. If the mass flow rate of propellant is $\dot{m}$ and the acceleration of the gravity is g_0, for F and $\dot{m}$ constant,

$$I_s = \frac{I_t}{m_p g_0} \ , \tag{2.5}$$

where m_p is the total effective propellant mass and the unit of I_s is in seconds [1, 2]. The amount of propellant needed for a particular mission is given by

the mass ratio MR which is the final mass m_f of the rocket (that is, after consumption of all usable propellant) divided by the initial mass m_o

$$MR = \frac{m_f}{m_0} \ . \tag{2.6}$$

Its value varies from 60% for some missiles to less than 10% for some unmanned launch vehicles. It is an important parameter in the analysis of flight performance [1].

The impulse to weight ratio which is the total impulse divided by the initial weight W_0 of the vehicle plays almost the same role as the mass ratio. Again, a high value indicates an efficient design. If we maintain the assumption of constant thrust,

$$\frac{I_t}{W_0} = \frac{I_t}{\left(m_f + m_p\right) g_0} = \frac{I_s}{\frac{m_f}{m_p} + 1} \ , \tag{2.7}$$

the thrust to weight ratio $\frac{F}{W_0}$ expresses the acceleration that the engine can provide to its own loaded propulsion system.

The power of the jet P_{jet} , which is the power carried by the ejected matter is given by

$$P_{jet} = \tfrac{1}{2} \dot{m} v^2 \ . \tag{2.8}$$

The thruster efficiency indicates how effective is the conversion of the input energy into the kinetic energy of the ejected matter [1, 3]

$$\eta_T = \frac{P_{jet}}{P_0} = \frac{\dot{m} v^2}{2 P_0} \ . \tag{2.9}$$

The specific power is the power per unit mass of the total propulsion system including the power supply [1, 3]

$$\alpha = \frac{P_0}{m_0} \quad . \tag{2.10}$$

In equations (2.9) and (2.10), P_0 is the total power produced by the power supply, and m_0 is the initial mass of the vehicle including the power supply. α is one of the most important parameters of a space vehicle with a separate power source. Larger values mean a larger power output per unit mass. If we assume that an electrically propelled space vehicle operates at a constant power level, this power level must be the highest possible for which its power producing plant is designed [3].

Another very important parameter of an ion engine is the ion source [3]. Requirements for the ion source are:

High power efficiency: it means that the total energy required for producing an ion should be as small as possible. E_{ion} is obtained by dividing the total power input into the ion source by the number of ions leaving the power source per second. Note that the ionization energy which is the energy required to detach one electron from an atom is only an insignificant part of E_{ion}. For present ion sources it ranges from between a few hundred and a few thousand electron volts per ion [3].

Propellant utilization: it is also called mass efficiency and is defined as the ratio of the mass flow of ions from the ion source, $\dot{M}_{out}^{+}$, and the mass flow of propellant into the ion source, $\dot{M}_{\text{int}}$,

$$\eta_M = \frac{M_{out}^{+}}{M_{\text{int}}} \quad . \tag{2.11}$$

A value of η_M close to unity is desirable as it shows that the biggest part of propellant entering the ionization chamber has been ionized. The effective thrust and terminal velocity of the vehicle are very much influenced by the propellant utilization as follow

$$F' = \eta_M F \qquad \text{and} \qquad u' = \eta_M u \,.$$

Here, the primed values are the effective ones [3].

Beam spreading: When the particles leave the acceleration chamber, they spread, because of the repulsive forces between them. If the spread angle of the plume is θ_m, the total thrust is given by

$$F = \frac{F_0}{2}\left(1+\cos\theta_m\right) \,. \tag{2.12}$$

Here F_0 is the thrust in the case that all particles leave the chamber parallel to the axis.

2.2 Existing systems

Space propulsion systems may be classified according to the means by which the propellant is accelerated. So there are thermodynamic propulsion systems in which the propellant is heated to a high temperature and accelerated through a nozzle, and electromagnetic systems, where the propellant is ionized and then accelerated with the aid of electric and or magnetic fields. We next discuss some thermodynamic systems used in heavy-lift launchers and then introduce some electrodynamic propulsion systems.

2.2.1 Thermodynamic systems

The two important forms of thermodynamic propulsion use chemical or nuclear energy for heating the propellant and then expand it through a nozzle. In the chemical rocket the energy is usually obtained by burning a fuel with an oxidant. Here the propellant may be solid or liquid.

2.2.1.1 Solid propellant rockets

A solid propellant rocket motor consists essentially of a propellant in a container fitted with an expansion nozzle and igniter. The two main classes of propellant used are termed double-base and composite. In the composite case, the oxidizer is a solid crystalline material such as ammonium. And in the double-base the system is mainly nitroglycerine and nitrocellulose in a gelatin form [13]. Solid propellant rockets are mostly used for military purpose and some launchers. Here follows a typical solid propellant motor.

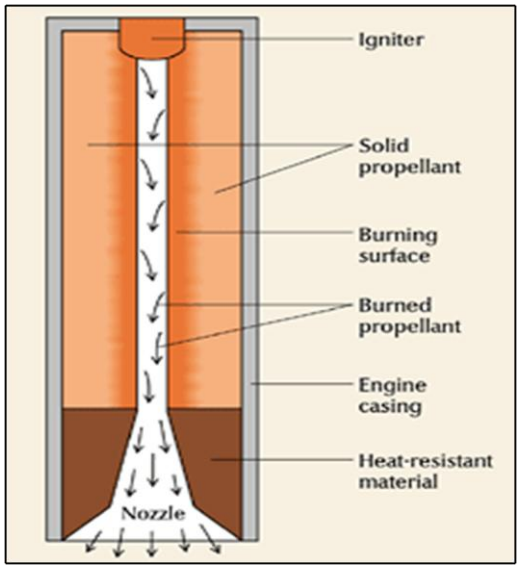


Figure 2.1: a typical solid rocket motor [14]

2.2.1.2 Liquid propellant rockets

In liquid propellant rockets, the propellant is carried in a liquid phase. There are some variant types, principally the one described as “pressure-fed” in which the liquid propellants are carried in tanks of a relatively heavy construction, from which they are displaced into the combustion chamber as gas at high pressure. Rockets described as “pump-fed” have lighter propellant tanks, and the propellants, stored at a low pressure, are fed into the chamber by mechanical pumps which are usually turbine driven. Also, a very large variety of liquid propellants may be used. In principle, any liquid capable of an exothermic chemical reaction yielding mainly gaseous products may be regarded as potential liquid rocket propellant. In general, liquid propellant rocket systems offer some advantages of higher performance when compared with solid propellants [13, 15].

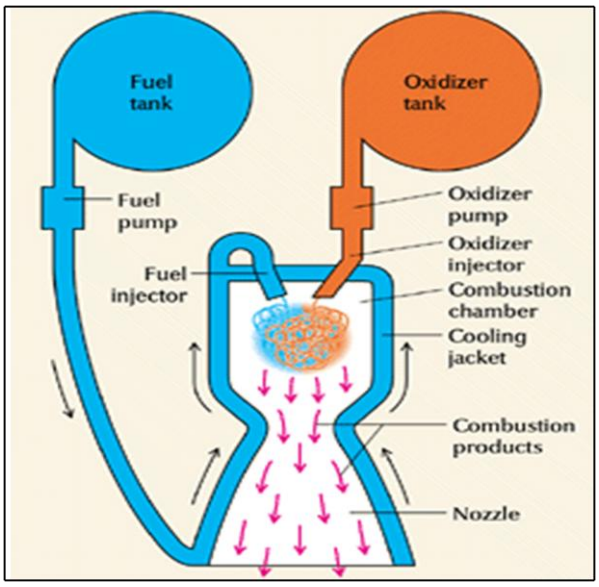


Figure 2.2: a typical liquid propellant rocket motor [14]

Both solid and liquid propellant rockets can achieve an exhaust velocity of up to 4km/s and thrust of up to $10^6\ N$ [10, 15]. Because the exhaust velocity is so low, chemical rockets would demand unachievable mass ratios for a real payload. That is

why all present launching vehicles are constructed from multistage rockets. Here the vehicle is made of many motors lifting a payload. See figure 2.3

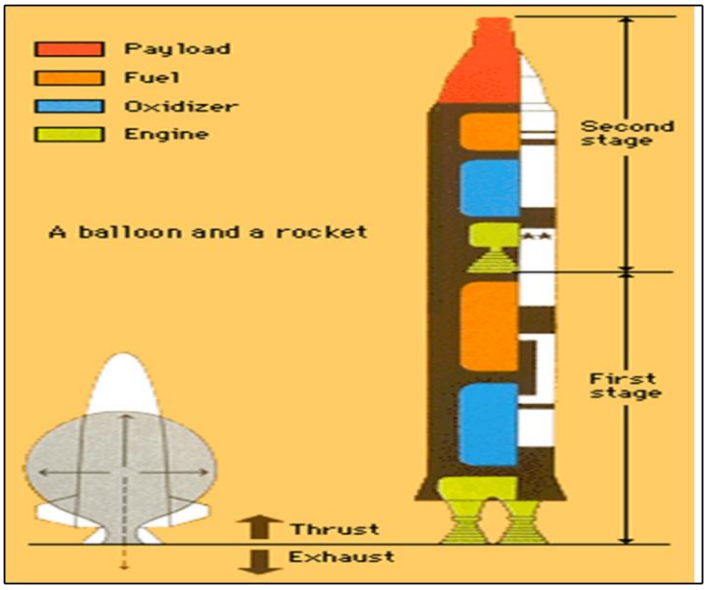


Figure 2.3: schematic of a two-stage rocket [14]

The fact that liquid propellant rockets are reusable makes them more economical for launchers. In figure 2.4, we demonstrate some launch vehicles used to carry space probes, artificial satellites and even people into the outer space.

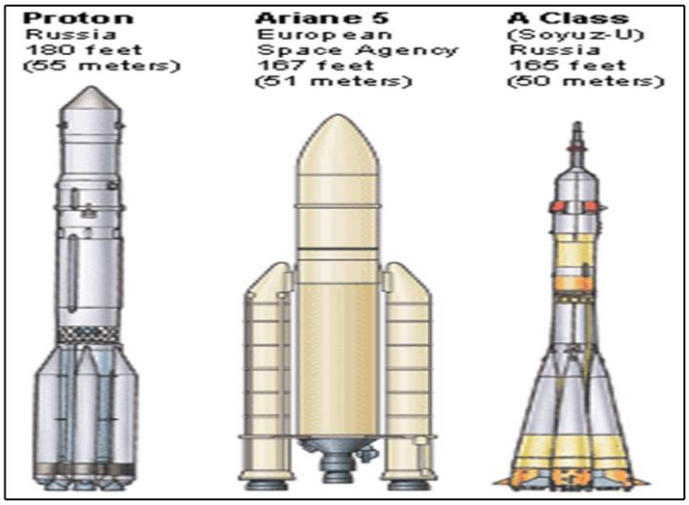


Figure 2.4: Some famous European launchers [14]

2.2.1.3 Nuclear Rocket

Aside from the chemical rocket, another type of thermodynamic rocket is the nuclear rocket in which the propellant is heated by passing it through a nuclear reactor. The most common propellant is hydrogen. The reactor can have a solid, liquid or gaseous core. The solid core fission reactor was used in 1955 by the USA in the NERVA program, using a graphite-based solid core homogeneous reactor. This has operated for as long as one hour at power levels of about 1000 megaWatts and exhaust temperatures of about 2000^{o} C [10, 15]. In figure 2.5 below a schematic of this concept is shown.

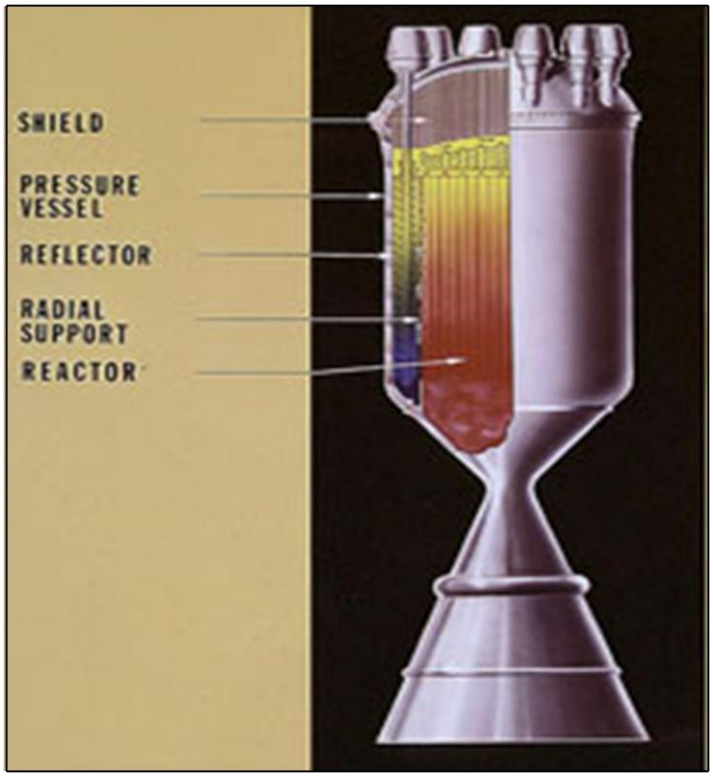


Figure 2.5: concept of the NERVA engine reactor [10]

Improvements can be made by reducing weights, increasing operating times, higher powers and higher temperatures. One factor limiting the temperature here is the melting point of the core material, where this can be overcome by using a liquid core reactor. This concept is mostly theoretical, this is also the case with the gaseous

core fission reactor in which exhaust velocities of 15 to 25km/s can be expected. There is also the possibility of using a gaseous fusion reactor, using the Deuterium-Deuterium or the Tritium-Deuterium reactions [13]. Here exhaust velocities around 40km/s can be expected.

2.2.1 Electrodynamics systems

2.2.1.1 Arc jet

When moving from thermodynamic to electrodynamic propulsion, one can take a "bridge" called Arc propulsion, in which the propellant is heated electrically and then expanded through a nozzle. Since the heating method is not restricted with regard to material limitation, temperatures of the order of 20 000K can be achieved, allowing a substantial increase in the propellant enthalpy and thus large exhaust velocity. Figure 2.6 is the 1kW hydrogen arc jet (NASA) in operation at the University of Michigan's Plasmadynamics & Electric Propulsion Laboratory (PEPL) [16]

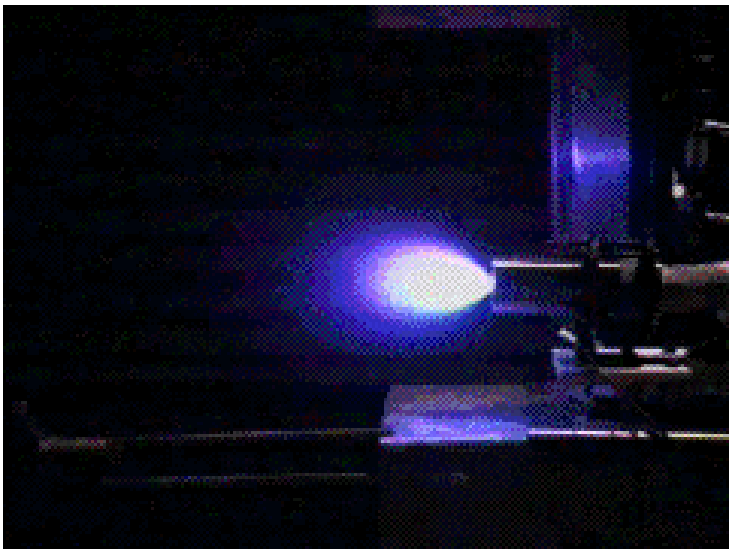


Figure 2.6: 1 kW hydrogen arc jet plume [16]

Thermodynamic rockets in general, and chemical rockets in particular, are energy limited, since the quantity of energy that can be released during combustion

is limited by the fundamental chemical behavior of propellant materials. If on the other hand, a separate energy source is used, much higher propellant energy is possible. But the issue of temperature limitation of the solid walls, that can only be solved by direct electrostatic or electromagnetic propellant acceleration (without raising the fluid and solid temperature [17]) remains.

The two most important forms of electrodynamic propulsion systems are the electromagnetic and electrostatic. Since in electrodynamic systems the acceleration of the propellant occurs without any raise in temperature, there shouldn't be any limitation to the energy that could be added to the propellant.

2.2.1.2 Electromagnetic thrusters

For this type of propulsion system, the propellant is ionized or heated into a plasma state and submitted to an electric and/or magnetic field [1]. Being in the plasma state, the propellant flow is neutral, and when submitted to the combined action of an electric and magnetic field perpendicular to each other, the positively and negatively charged particles will experience a force in the same direction. This force is proportional to the charge, but independent of the particle mass [6]. These systems do not need the neutralization of the exhaust as it is already neutral. Electromagnetic systems can produce an exhaust velocity considerably higher than those of electro-thermal devices, and thrust densities much larger than those of electrostatic thrusters (though more complex and less tractable than either of these alternatives [6]) of the many different electromagnetic propulsion systems, Some examples are shown in figures 2.7, 2.8 and 2.9

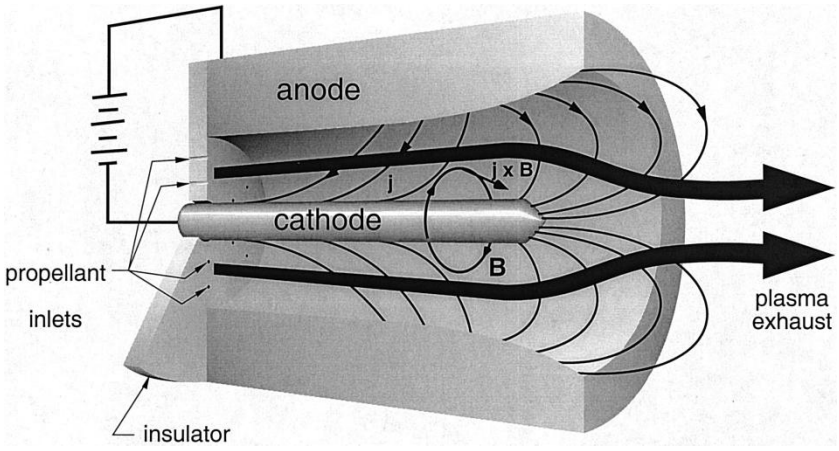


Figure 2.7: schematic of a magnetoplasmadynamic thruster. Here, gaseous propellants are introduced into the upstream portion of the channel, where after they are ionized by passage through an intense, azimuthally uniform electric arc standing in the interelectrode gap. If the arc current is high enough, its associated azimuthal magnetic field is sufficient to exert the desired axial and radial body forces on the propellant flow, directly accelerating it downstream and compressing it toward the centerline into an extremely hot plasma just beyond the cathode tip. Subsequent expansion of this plasma, along with the direct axial acceleration, yields the requisite exhaust velocity. [6]

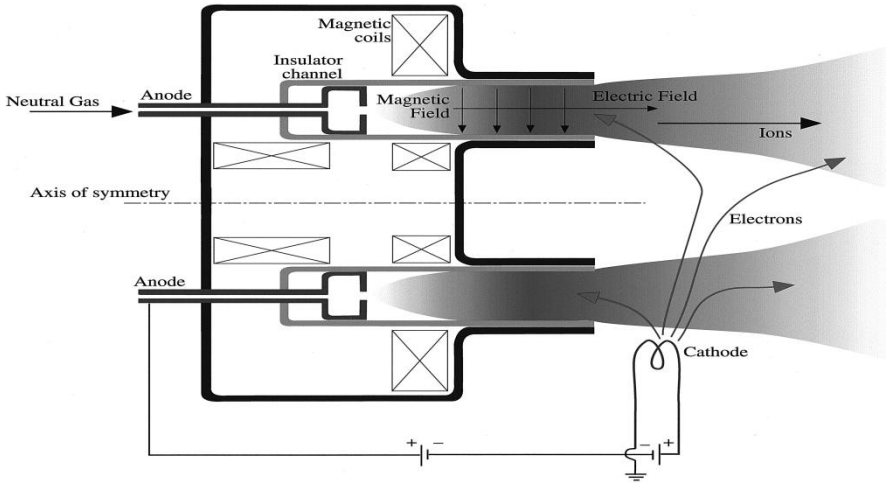


Figure 2.8: schematic of a Hall Effect thruster with an extended insulator channel (stationary plasma thruster, or SPT), showing the external cathode, the internal anode, the radial magnetic field, and typical particle trajectories [6]

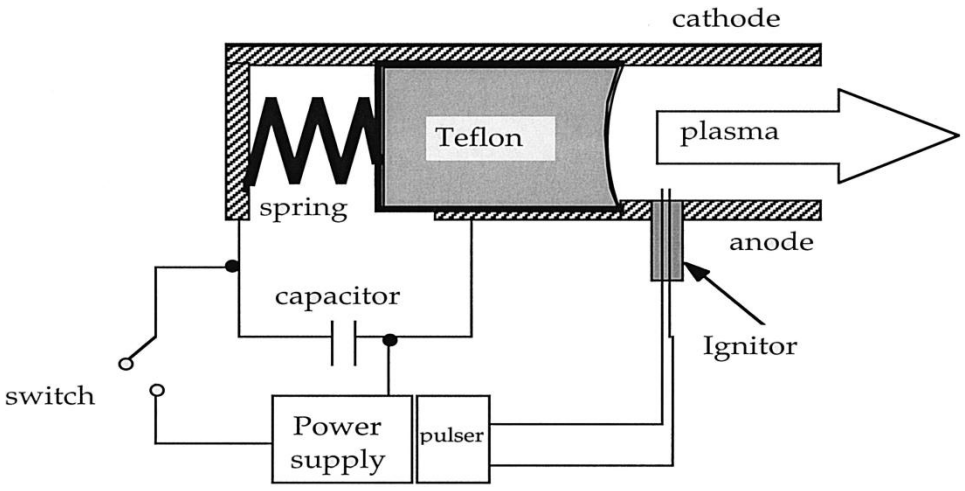


Figure 2.9: schematic of an ablative pulsed plasma thruster (APPT). The surface of a polymer block (most commonly Teflon) is successively eroded by intermittent arc pulses driven across its exposed face, and the ablated material is accelerated by a combination of thermal expansion and self-field electromagnetic forces. [6]

2.2.1.3 Ion Engine

In ion engines, the acceleration of the propellant is achieved by means of an electrostatic field. For this to happen, the propellant must be ionized. Ionization is achieved by electron bombardment, radio frequency, electron cyclotron resonance or Cesium contact ionization [7, 9]. Electron bombardment, which is one of the most efficient has improved much since the first laboratory test in 1960, to the first successful flight on the NASA's Deep Space I in 1998 [4] . So the ion production cost has increased from 400-600 eV for Hg at an 80% mass utilization fraction to some 116eV in Xenon at the same utilization [9]. Since the acceleration does not rely on heating, very high exhaust velocities can be obtained.

The exhaust beam which is positively charged needs to be neutralized in such a way so as to avoid charge build up on the spacecraft. In many ion engines this is done by an external cathode emitting an electron beam at the same rate as the ion beam [4, 7, 9]. This is illustrated on figure 2.10

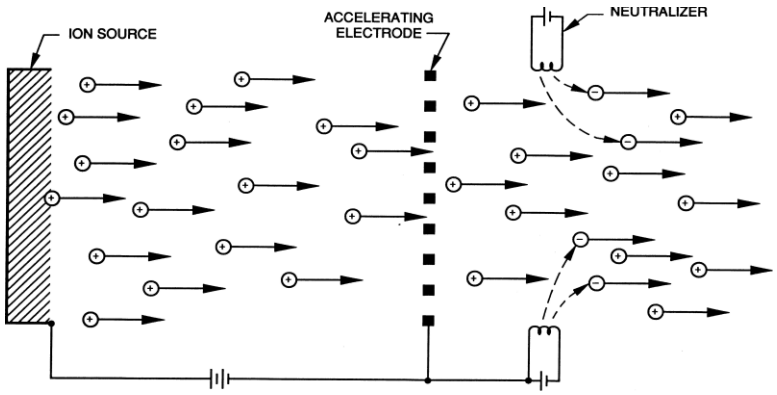


Figure 2.10: ion thruster schematic [6]

An ion engine consists of three major components: a discharge chamber in which the propellant ionization takes place, an ion acceleration system which extracts the ions from the discharge chamber and accelerates them to the exhaust velocity, and a neutralizer which injects electrons into the positive ion beam to provide space-charge and current neutralization. A complete system also includes the propellant tank, propellant feed system and an external power supply [1, 4, 9, 18]. Figure 2.11 shows a simple schematic of an ion engine.

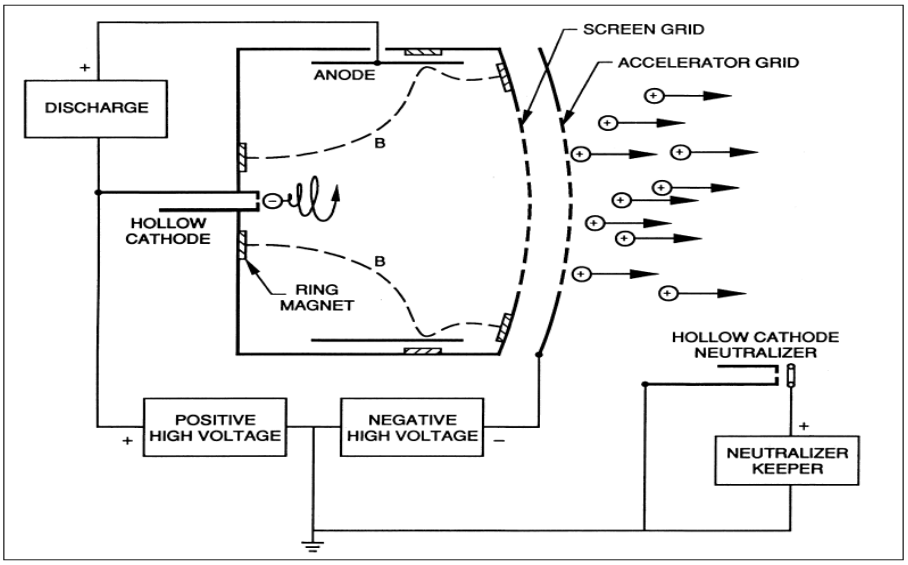


Figure 2.11: Schematic of an electron bombardment ion engine [6]

Heavy atoms of the propellant are fed into the discharge chamber where the ionization takes place. The gas contained in the chamber is weakly ionized but the small electric field inside the chamber acts to extract ions preferentially to neutrals. So as a first approximation we may assume that only electrons and ions leave the chamber. Ions are accelerated by a strong potential difference applied between perforated plates and this same potential keeps the electrons from also leaving through these grids. These grids are designed to reduce ion beam divergence due to space charge effects. The electrons are collected by an anode which in many cases is just the walls of the discharge chamber, where these electrons must be ejected to join the ions downstream of the accelerating grid. To do this, electrons must be injected into the beam by some electron emitting device which usually consists of a thermionic cathode which emits electrons when heated or by a plasma bridge [1, 4, 9, 18]. The reaction to the momentum flux of the plasma beam is the thrust of the device.

Ideally, there is no current flow through the external circuit connected to the accelerator grid, as it should not collect any ions or electrons. So its power supply only applies a static voltage. All the electrical power consumed by the device is that of the neutralizer, as it must pass an electron current equal in magnitude to the ion beam current and must also have an acceleration voltage across its terminals [1, 4, 9]. Figures (2.12) and (2.13) below show the Deep Space I spacecraft and its NSTAR ion engine, which is a 30cm ion thruster able to produce a thrust of 20 to 92 mN and a specific impulse of 3100 s. Using 81.5 kg of Xenon propellant, it can provide thrust for 20 months [19]

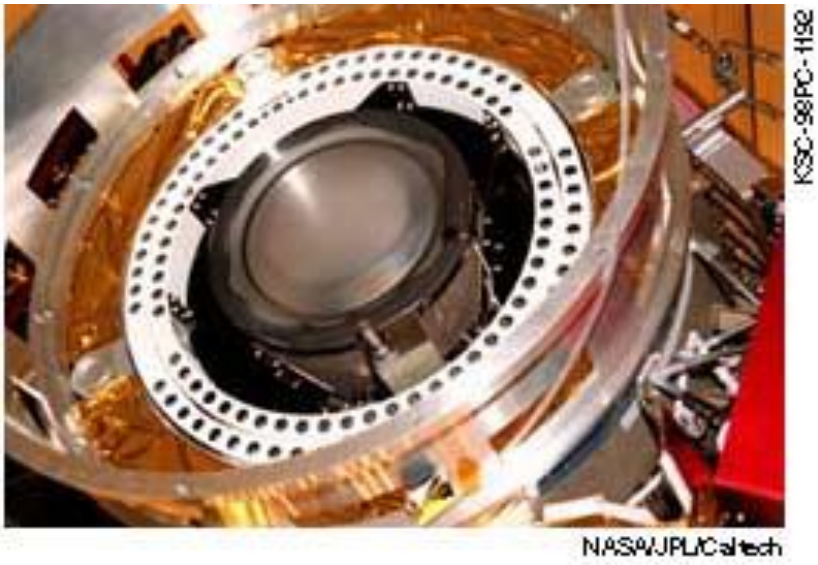


Figure 2.12: close up-view of the NSTAR ion engine [19]

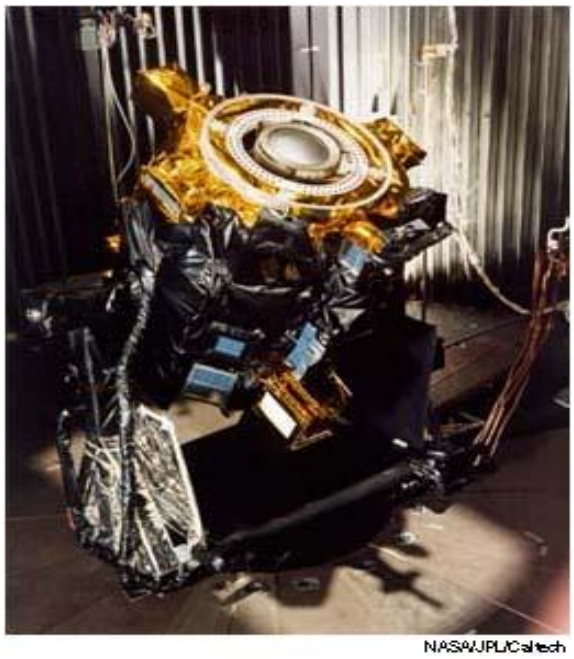


Figure 2.13: Deep Space I spacecraft during testing [19]

Electrical rockets are thrust density limited and differ fundamentally from chemical rockets. The latter rockets are used to take a payload into a specific orbit around the earth and the former keeps it in orbit or can take it into another orbit or interplanetary transfer. It should be noted that ion engines have a low thrust density (thrust per unit exit area), this being due to the fact that there is a limit to the amount of current and hence mass flow which can be extracted between the acceleration grids [1, 4, 7, 6]. This makes the ion engine able to operate only in low pressure or in a vacuum. Ion engines can theoretically provide the highest specific impulse of all electric propulsion systems, which can be within the range of 1000-10000s. Thrusts of between 0.01 and 1000mN, efficiencies of up to 90% and exhaust velocities of 30-200km/s can also be obtained [1, 6]. As there is no perfect system, ion engines have many problems that must still be addressed. Here are some of them:

- Erosion due to the impact of ions with the accelerating grid
- Use of external electrical power for ionization, acceleration, and neutralization which increases the mass of the thruster.
- High cost of ionization due to recombination in the discharge chamber
- Beam divergence due to the effect of the space charge
- Incomplete ionization of the propellant present within the discharge chamber

After this overview of existing propulsion systems we shall now say a word on some ionization mechanisms and the Corona Discharge since the theoretical analysis of this new thruster relies on such concepts.

Chapter 3

Corona Discharge and the Proposed Concept

3.1 Corona Discharge

We next discuss concepts related to Corona discharge such as the ionization and plasma.

The term “Plasma” was used for the first time in 1927 by Irling Langmuir to describe ionized gases because the way electrons, ions and particles flow in these gases is the same as blood plasma. Plasma science has developed and is today a field of its own and is used in industry to manufacture semiconductors, medical products etc, it is also used in space propulsion [5, 11].

3.1.1 Some properties of Plasma

In order to talk about the properties of plasma, we must remember the five states of matter:

- the three well known (solid, liquid and gas)
- BoseEinsteinnium Condensate (BEC) (state of matter predicted by A. Einstein using mathematical formulations developed by S.N. Bose in the early 1920’s. This state occurs when atoms, cooled down to a fraction of a degree above the absolute zero, coalesce together to form a super atom that behaves as one entity [11]).
- Plasma is a gaseous mixture of free electrons and ions that have a high mean kinetic energy. Neutral plasma contains an equal number of positive and

negative charge carriers so that the net charge is zero. Because of the presence of the charge carriers, plasma is an electrically conductive fluid. Plasma is strongly influenced by electric and magnetic fields through Coulomb and Lorentz laws.

3.1.2 Ionization mechanism

Ionization is a physical process of converting an atom or molecule into an ion by adding or removing charged particles as electrons or other ions. There are many ways of doing this:

- **Surface ionization**

In this method, an alkali vapor passes over a metallic surface and if the work function of the metal is higher than the first ionization potential of the vapor, the valence electrons of the vapor are caught by the surface [1, 3, 18]. Unfortunately, this occurs only for a few numbers of propellants, notably Alkali metals, which are very corrosive and toxic.

- **Photo-ionization**

If gas molecules or atoms are illuminated by photons of frequency ν, providing the energy hν, the gas can be ionized if the energy of the photon beam is greater than the ionization energy of the gas. Photo-ionization can occur by steps; meaning that a photon of energy less than the ionization energy can take the atom to an exited state and another photon comes to ionize that exited atom. This occurs mostly when the exited state is meta-stable [12, 20]. Note that the same thing can happen with X-Rays and Cosmic Rays [20].

- **Thermal ionization**

From the kinetic theory of gases we know that at high temperature the average velocity and the kinetic energy of gas atoms are very high. As such collision between the atoms can cause ionization or excitation. In the case of excitation the atom can

recover its initial state by emitting radiation. This radiation can excite or photo-ionize another atom. Since all this happens because of the thermal condition of the gas, the phenomenon is known as thermal ionization. It is worth noting that this phenomenon does not occur easily. For instance, in the earth's atmosphere at room temperature, one ionizing collision will occur every 10^{500} years [20]. Thermal ionization depends on the ionization energy of the gas: cesium vapor, which has the lowest ionization energy, will have one ionizing collision out of 2000 collisions at a temperature of 10,000K [20].

- **Ionization by electron bombardment**

Here electrons are emitted by a thermionic cathode into the ionization chamber, where they collide with neutral propellant to ionize its molecules [1]. Ionization only occurs if the kinetic energy of the electron is equal or greater than the ionization potential of the propellant [12, 20]. The chamber walls that constitute the anode attract the electron and an external magnetic field applied to the chamber causes the electron to gyrate around inside the chamber in order to increase the distance traveled by it before reaching the anode and so increasing the kinetic energy and ionization probability [1]. This method, so far, is the most developed and has been used in many space-crafts such as the Deep Space I Ion Engine [4].

3.1.3 Field intensified and corona ionization

Consider two parallel plates connected to an external power supply and sealed inside a glass container as shown in figure 3.1 below [18].

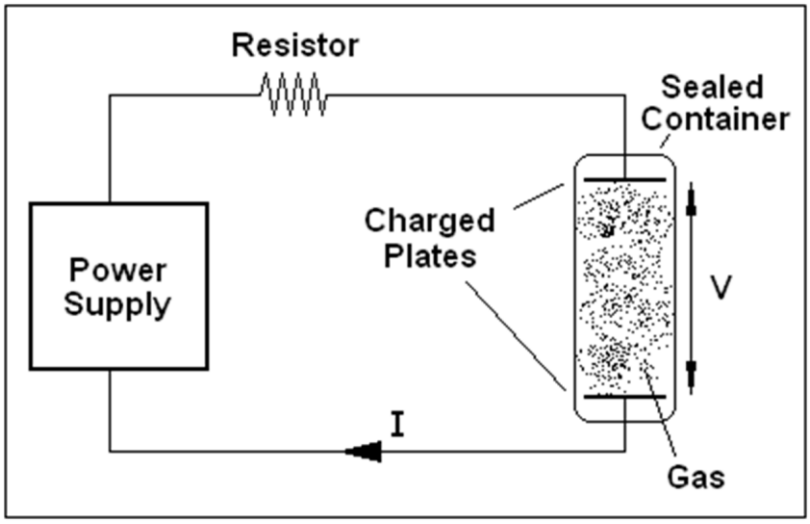


Figure 3.1: schematic of a typical gaseous discharge circuit

As a gas is introduced into the container, due to thermal agitation, the gas molecules are submitted to a random motion [12]. This motion leads to collisions between them and there is a probability of ionization by collision. Without any electric field the rate of electrons and positive ions is counterbalanced and a state of equilibrium exists. When we apply a voltage the current in the circuit increases with the increase in voltage until a value $I_{0,}$ known as the saturation current, is reached, where it remains nearly constant over a wide voltage range. If one keeps increasing the voltage, a voltage is reached where the current will increase exponentially above the value I_0 [18, 21]. The current as a function of the voltage is given figure 3.2.

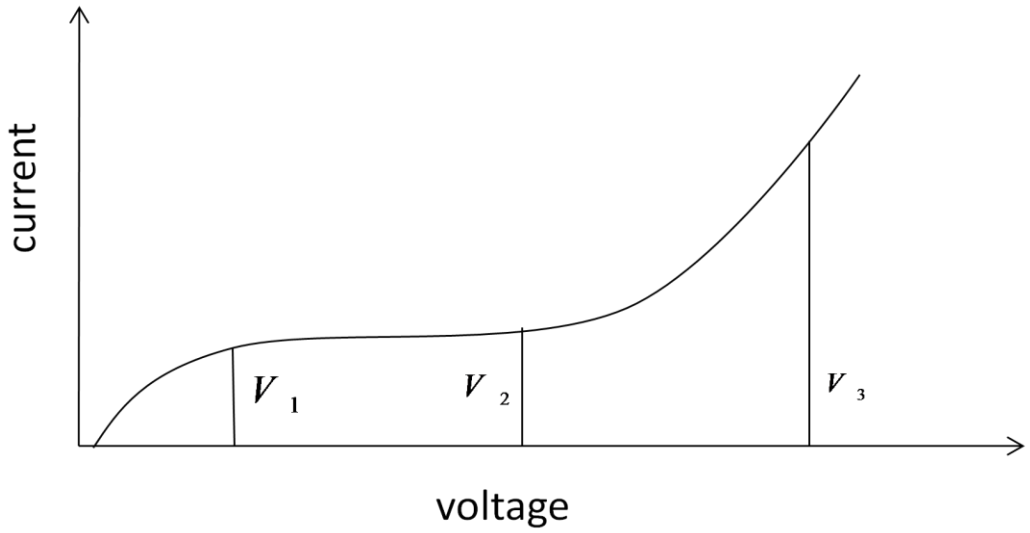


Figure 3.2: current-voltage relationship for a gas discharge process

When the power supply is 'on' the plates become oppositely charged and hence an electric field is established between them. The electrons are accelerated and gain kinetic energy by moving along the field direction. If the field is strong enough and the mean free path of electrons is large electrons gain energy that can result in ionization by collision with neutral molecules in the gas. Any ionizing collision produces 2 electrons: the initial one and the one released by the atom. These two electrons are ideally accelerated and can produce four which produce eight, then sixteen and so on. This is an exponential proccess which describes the portion of the curve between V_2 and V_3. To explain this current increase Townsend introduced a quantity α, known as Townsend's first ionization coefficient, defined as the number of electrons produced by an electron per unit length of path in the direction of the field [21, 22, 23]. If n is the number of electrons at a distance x from the cathode, the increase in electrons dn in the distance dx is given by $dn = \alpha n dx$

By integrating over the distance d between the plates one obtains

$n = n_0 e^{\alpha d}$,

where $e^{\alpha d}$ represents the number of electrons produced by one single electron in covering the gap distance [22, 23], such that the current in the circuit is given by $I = I_0 e^{\alpha d}$, α depends on the strength of the electric field and on the gas pressure by the relation $\frac{\alpha}{P} = f\left(\frac{E}{P}\right)$.

The quantity $\frac{\alpha}{P}$ gives the ionization efficiency. Figure 3.3 below shows a typical $\frac{\alpha}{P}$ vs $f\left(\frac{E}{P}\right)$ curve were the point $B/2$ and B refer to a constant in the exponent of Townsend's approximate relation giving the point of inflection and tangent to the curve from the origin [23].

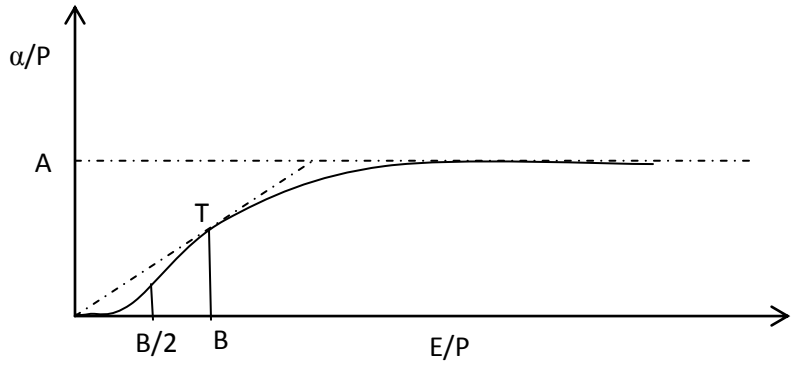


Figure 3.3: typical $\frac{\alpha}{P}$ vs $f\left(\frac{E}{P}\right)$ curve

To increase the current flowing through the circuit one can initiate with some free electrons, known as triggering electrons that can be produced either by use of radioactive elements or UV light, which extracts some electrons from the cathode by photoemission. The most used method is UV light as it is adjustable and one can control it better than the emission of radioactive elements [23].

3.2 Proposed Concept

We next introduce an electric propulsion system based on the Corona Ionization mechanism that we will develop a first approximation mathematical model in the theoretical part of this project. The system is called the "Corona Ionization Space Propulsion System" (CorIon) [18]. Here, the main body of the thruster is a sharp electrically conducting, hollow needle. In operation the propellant tank feeds propellant through the hollow needle, which is maintained at a very high potential by an external power source. The propellant exits through the sharp tip into the very strong electric field at that point. Corona ionization takes place in the strong field region, stripping electrons away from some propellant molecules. The electrons are attracted by the positively charged needle tip, where they further ionize propellant molecules by collision. The positive ions are repelled from the needle and collide with neutral molecules exiting the needle. Collisions of these fast ions with neutral molecules increases the overall speed at which the propellant stream exits the needle, effectively "heating" the exhaust plume in the direction away from the thruster. This mechanism provides the thrust. The figure 3.4 below shows neutral gas and ions exiting the needle tip

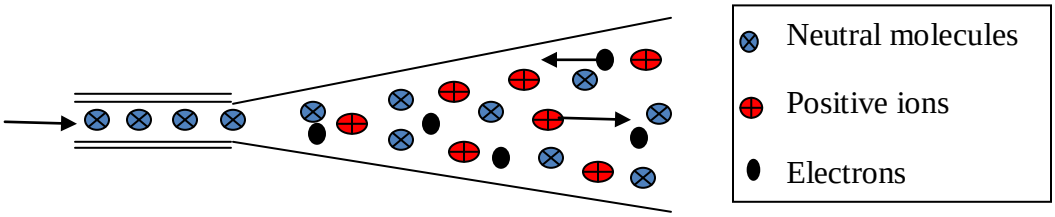


Figure 3.4: schematic of the plume exiting the positively charged needle

Here are the main differences between this system and the conventional ion engines:

- There is less erosion since there is no accelerating grid and collisions occur mainly between electrons and the needle, which causes less erosion.
- Positive ions will still be attracted to the negative terminal, but we expect there to be fewer, since the field close to the needle dominates. Also, the negative terminal is so far away that it can be sacrificial.
- The ionization and the acceleration system are coupled, reducing the system mass, size and complexity.
- Very large accelerating voltages could be used.
- The ionization cost could be reduced, since the recombination loses will be much lower as no chamber walls exist.

3.3 Basic requirement of the system

3.3.1 The Needle

Shape: We need to use a very sharp needle to reduce the potential required to produce a very strong electric field. Also the needle must be entirely insulated to ensure that ionization only takes place at the needle tip. The cross-section of the needle needs to be symmetric to ensure that the gas leaves smoothly and to minimize beam divergence. For high beam divergence part of the thrust produced will not act in the direction opposite the motion, reducing the efficiency.

Material: The outer surface of the needle can be damaged by electron bombardment as well as by the heat generated. So the material must be heat and erosion resistant.

Size: The idea is to obtain a high enough gas density that results in suitable ionization at the needle tip. If the gas exit density is too low the electron mean free path is too long and few ionization events occur. A small inner diameter is desirable, but this in turn increases the friction of the gas molecules inside the needle and may

change flow characteristics. The outer diameter should also be small for the point charge approximation. We further know that the Corona onset voltage varies with the radius of the electrode [24]. Table 3.1 below shows how the potential gradient (electric field) varies with diameter and the material of the conductor.

Table 3.1: Variation of the electric field with the electrode diameter for some materials [24]

Diameter in cm	Electric field at needle tip (kv/cm)	material	Diameter in cm	Electric field at needle tip (kv/cm)	material
0.0196	116	Tungsten	0.2043	59.0	Copper
0.0343	99	Copper	0.2560	57.0	aluminum
0.0351	94	Copper	0.3200	54.0	Copper
0.0508	84	Aluminum	0.3230	50.5	Copper
0.0577	82	Aluminum	0.5130	49.0	Copper
0.0635	81	Tungsten	0.5180	46.0	Copper
0.0780	76	Copper	0.6550	44.0	Copper
0.0813	74	Copper	0.8260	42.5	Copper
0.1637	64	Copper	0.9280	41.0	Copper
0.1660	64	iron			

The corona onset voltage is also a function of the electrode radius as can be seen on the graph below, figure 3.5.

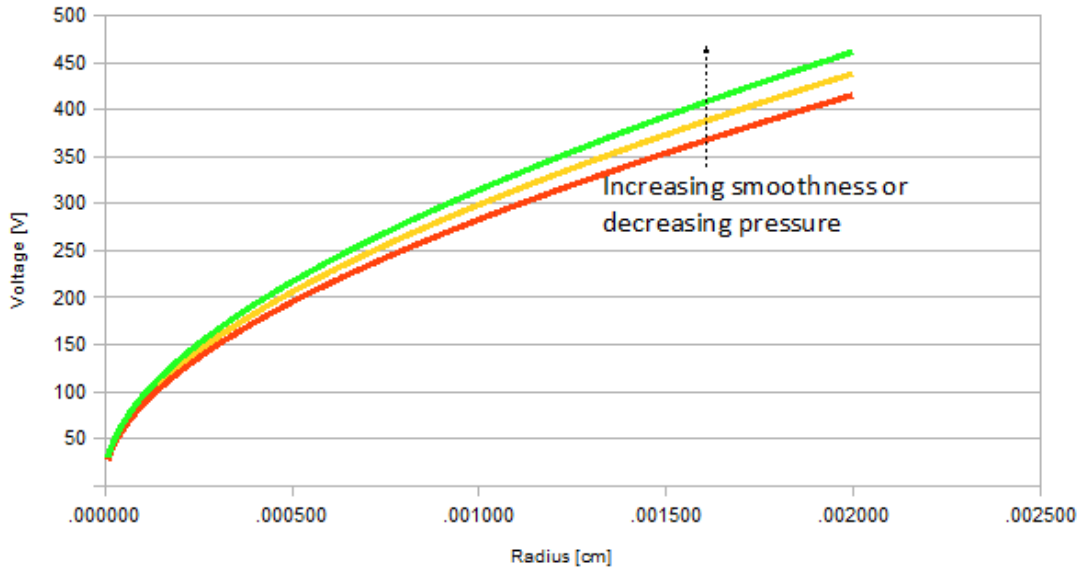


Figure 3.5: Corona onset voltage variation with electrode radius [25]

3.3.2 The propellant

Many things have to be taken into account for the choice of the propellant. Here follows some of the more important factors:

Purity: A high purity refers to a low amount of other gases. Corona ionization is strongly influence by the amount of impurity in the gas considered. The idea is to have a gas as pure as possible, which increases cost.

Molecular mass: in a conventional ion engine, a higher molecular mass increases the thrust produced by the system through equation (2.1)

Ionization energy: the ionization energy is of great importance because we want to use less energy for ionization so that the larger part of the energy goes into the acceleration of ions.

Another requirement is to choose a non corrosive propellant. So the choice should be amongst noble gases. Figure 3.6 shows how the ionization energy of noble gases changes with the atomic number, identifying Xenon as a good candidate

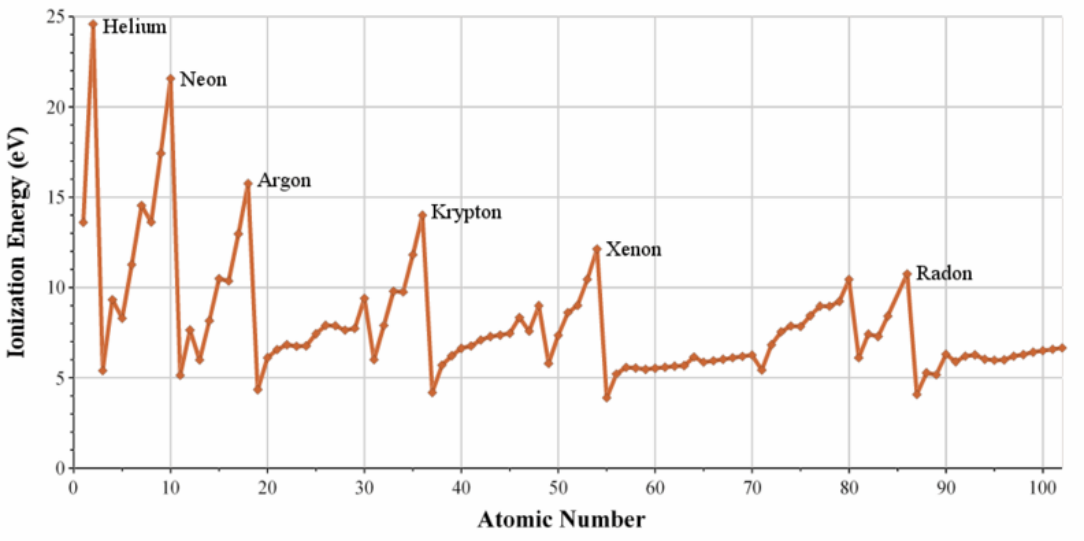


Figure 3.6: Ionization energy of different noble gases [26]

3.4 Effect of the incomplete ionization of the propellant

Following equation (2.11), a complete ionization of the propellant is desirable. But the CorIon will be seen to have a low ionization rate, in the order of 1 % of gas flow. We want to compare two systems, one in which the propellant is completely ionized and another partially ionized. The example below uses a homogeneous electric field for simplicity which should illustrate the point.

We consider two tubes of length *d* and cross-sectional area *A*. Inside and along the tubes is a homogenous electric field generated by a potential difference *V*. In one tube, called *system 1*, all the neutral propellant entering the tube is ionized and ejected on the other side with a final velocity which was attained through unimpeded acceleration. In the other tube, called *system 2*, there is only partial ionization, and the ions travel, on average, with some drift velocity due to regular collisions with neutrals. The figure 3.7 below is an illustration of the two tubes.

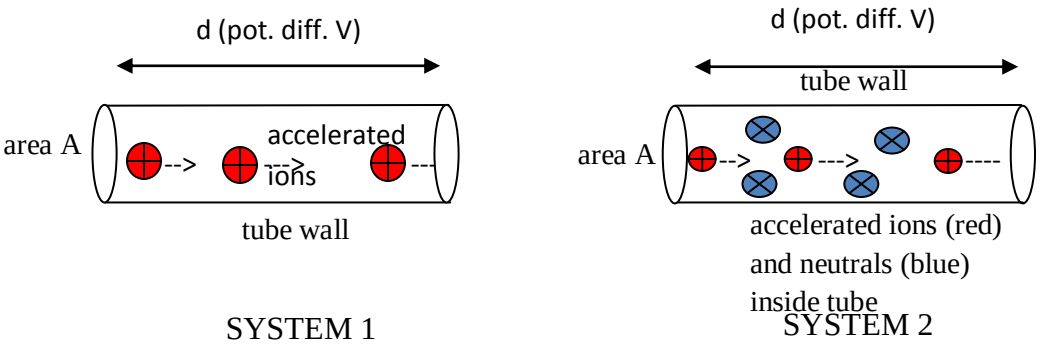


Figure 3.7: comparison of the two tubes (complete and incomplete ionization)

The force against the tube is given by the recoil of the electrostatic force applied in accelerating the ions. We consider a small cross sectional volume of the tube, *dV*, which contains a number of charges *Nq* (see figure 3.8), and which exerts a small force against the tube given by Coulomb's law.

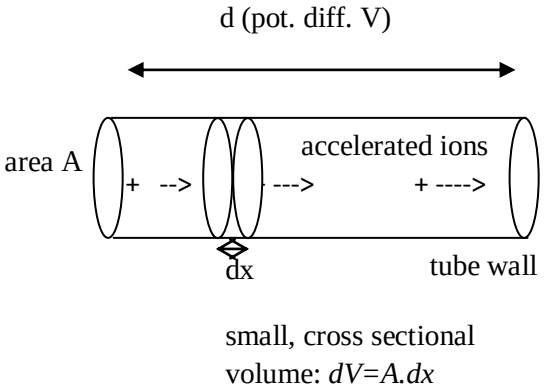


Figure 3.8: schematic of a cross sectional volume

Using the definition for total current given by $i = \rho_e(r).V(r).A(r)$ and further the fact that the charge density is $\frac{number\ of\ charges}{volume}$:

$$\rho = \frac{Nq}{A.dx},$$

such that

$$i = \frac{Nq}{A.dx}.V.A\ .$$

Or

$$Nq = \frac{i.dx}{V}\ .$$

This gives, for the infinitesimal force on the sliver:

$$dF = \frac{i.E.dx}{V}, \tag{3.1}$$

and for our systems, *i* and *E* are constants, while *v*, the velocity at a distance *x*, is a function of space for *system 1*.

The charges in *system 1* are accelerated by a constant force. Hence we may use

$V^2 = u^2 + 2ax$, with $a = \frac{Eq}{M}$ and the initial velocity is 0.

This gives for the final exit velocity v of the ions in system 1 after a distance *x*:

$$V = \sqrt{\frac{2Eqx}{M}}\ .$$

This allows us to obtain the charge density at that distance. q is the elementary charge and M the molecular mass.

Substitution of this into (3.1) yields

$$dF = \frac{i.E.dx}{\sqrt{\frac{2Eqx}{M}}}$$

$$dF = i.\sqrt{\frac{EM}{2q}}.x^{-1/2}.dx$$

Integration over the length *d* gives the total force by each sliver acting on the tube:

$$F_1 = i_1\sqrt{\frac{2EMd}{q}}.$$

and using $E_1\ d = V_1$, where we have opened the possibility of a different potential difference along the tube for the systems; we have

$$F_1 = i_1\sqrt{\frac{2V_1M}{q}}.$$

Which is the familiar expression for electric thrusters, namely

$$F = \sqrt{2P\dot{m}}\ .$$

Where F is the thrust, P the power and $\dot{m}$ the mass flow rate.

For system 2, the drift velocity is given by [12, 20]

$$V = const\ .\sqrt{E}\ .$$

Substitution into (3.1) and integration gives:

$$F_2 = i_2.\left(\frac{2}{K}\right)^{\frac{1}{4}}.\sqrt{\frac{V_2Md}{q\lambda}}$$

where $E_2.d=V_2$ was used.

We next want to ensure that we use the same rate of propellant consumption in both systems. This means that

$$\frac{i_1}{q} = \frac{i_2}{q} + \frac{\dot{m}}{M} \qquad (3.2)$$

i.e. the number of charged particles ejected in *system 1* is equal to the number of charged particles ejected of *system 2* plus the neutrals ejected. We may further write

$$\frac{\dot{m}}{M} = s\frac{i_2}{q}\,, \tag{3.3}$$

where s represents the ratio of neutrals to charged being ejected in *system 2*.

Equation (3.2) becomes:

$$\frac{i_1}{q} = \frac{i_2}{q} + s\frac{i_2}{q}\,,$$

or

$$i_1 = i_2(1+s)\,. \tag{3.4}$$

This relation needs to be substituted into the mean free path

$$\lambda = \frac{1}{n\sigma} = \frac{1}{\frac{\dot{m}}{MAv_e}\sigma} = \frac{1}{s\frac{i_2}{q}\frac{1}{Av_e}\sigma} = \frac{qAv_e}{si_2\sigma}\,. \tag{3.5}$$

Where v_e is the exit velocity, λ is the mean free path, n is the number density of neutrals and σ the scattering cross-section.

Using equation (3.3) above as *s* goes to zero, the formalisms of *system 1* and *system 2* should be identical, but they are not. This formalism is likely to be only accurate for values of *s* such that the mean free path is very much smaller than *d*.

These relationships ensure that the same amount of propellant is used in both systems, when they are implemented . Hence F_2 becomes:

$$F_2 = i_2.\left(\frac{2}{K}\right)^{\frac{1}{4}}.\sqrt{\frac{sV_2Mi_2\sigma d}{q^2Av_e}} = \frac{i_1}{(1+s)}.\left(\frac{2}{K}\right)^{\frac{1}{4}}.\sqrt{\frac{sMV_2i_2\sigma d}{q^2Av_e}}\,. \tag{3.6}$$

If we also wish to keep the power input the same for both systems, then we have $i_1V_1 = i_2V_2$. We therefore substitute for i_2V_2 in the square root above and obtain

$$F_2 = \frac{i_1}{(1+s)}.\left(\frac{2}{K}\right)^{\frac{1}{4}}.\sqrt{\frac{sMV_1i_1\sigma d}{q^2Av_e}}\,, \tag{3.7}$$

and now F_2 is written entirely in terms of variables used to write F_1, and any comparison between the two will be made at the same propellant consumption and electric power input. A comparison between the forces F_1 and F_2 can now be implemented by dividing them, which yields the final comparative relationship (at same power/propellant consumption):

$$\frac{F_2}{F_1} = \frac{1}{\sqrt{2}}\sqrt{\frac{s}{(1+s)^2}}.\left(\frac{2}{K}\right)^{\frac{1}{4}}.\sqrt{\frac{\sigma d}{Av_e}}\sqrt{\frac{i_1}{q}}\,. \tag{3.8}$$

From equation (3.8) one can see that the performance ratio of the two systems depends on choice of material (propellant, σ, and even q, the amount by which the propellant ionises), dimensions of the actual thruster unit (A and d) as well as operation parameters (v_e and i_1). The perfomance is an engineering question, since electrical properties (specifically resistence) of the system can adjust s, the ratio of neutral to charged particles ejected.

When equation (3.8) >1, *system 2*, using drag forces, produces more thrust at the same propellant utilisation and power than a system ionising completely, within the context of these descriptions.

For s large (>> 1, many more neutrals than charged), the above ratio is suppressed by roughly $s^{-1/2}$, while for small $s << 1$, it is suppressed by roughly $s^{1/2}$. An optimum is achieved at $s = 1$, when the number of neutrals equals the number of ejected ions, making the s-dependent ratio = ½ .

So the perfomance ratio:

- Depends on engineering factors that can favor incomplete ionization

- Does not take into account the ionization power, which favours incomplete ionization even more
- Can favour incomplete ionization for a chosen set of parameters.

After this short discussion we shall now move on to the theoretical analysis of the proposed concept.

Chapter 4

Electric field and Potential as Function of the Current

The thruster consists basically of a thin metal pipe with a sharpened tip, such as a hollow needle. The needle is electrically connected to a battery which keeps it at a high positive potential, and the cathode is at some other point, completing the field. In operation, the propellant tank feeds propellant through the hollow needle, which is maintained at a very high potential by the external power source. The propellant exits through the sharp tip into the very strong electric field there. Corona ionization takes place in the strong field region, stripping electrons away from some propellant molecules. Free electrons from the plume region are attracted and move towards the needle tip, where they further ionize propellant molecules by collision. An electron avalanche is thus created which collides eventually with the needle tip. The positive ions find themselves in a very strong electric field accelerating them away from the needle tip. If the emerging gas density is high enough, these ions will collide many times with neutral gas molecules in the plume. Collisions of these fast ions with neutral molecules increases the overall speed at which the propellant stream exits the needle, effectively heating the exhaust plume in the direction away from the thruster. This mechanism provides the thrust.

4.1 Exhaust plume description

The following diagram represents the exhaust plume

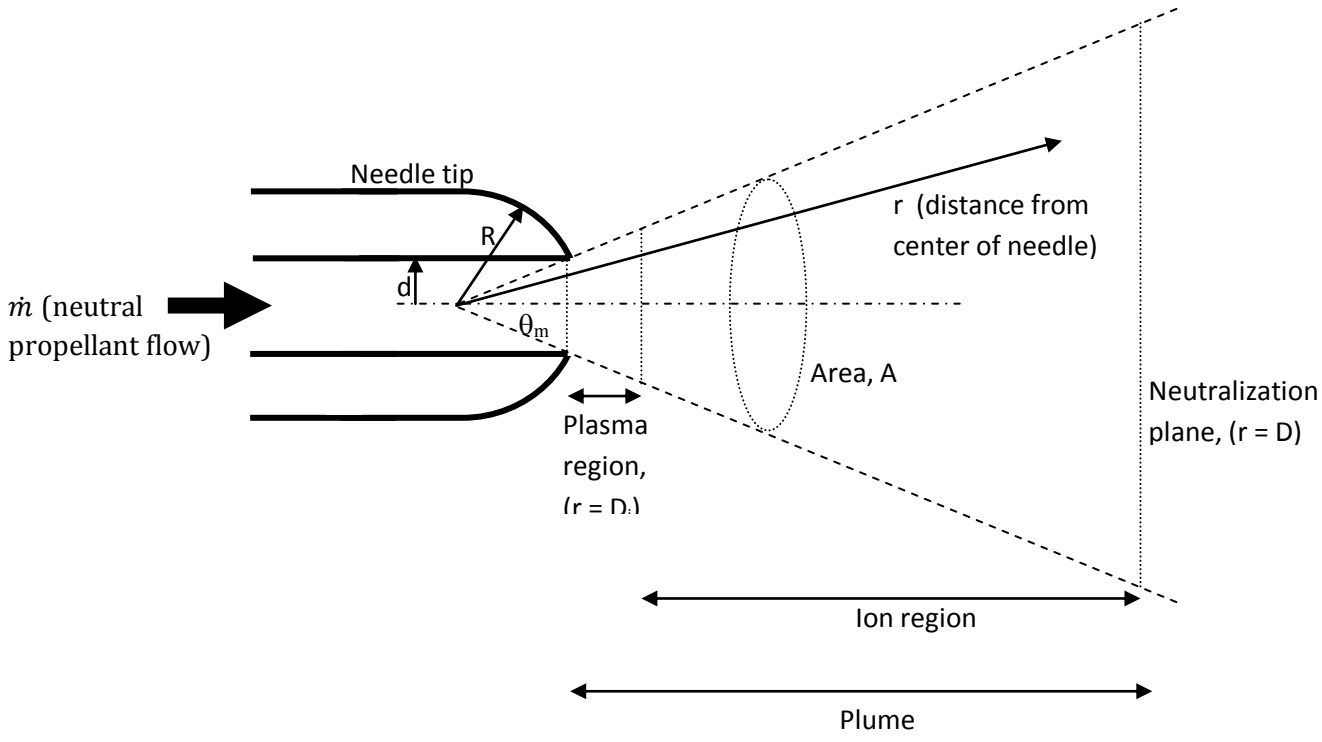


Figure 4.1: schematic of the exhaust plume

The exhaust plume can be divided into three regions with different physical properties:

- **Plasma region**

This region is where ionization takes place. Here there is a mixture of neutral atoms, electrons and positively charged ions. The net electric charge of this region is zero as the number of ions and electrons are similar. This region is so close to the needle tip that the two are taken as one and the same point which is the ionization region [23].

- **Ion region**

After ionization in the plasma region, electrons are attracted by the positively charged needle and the ions are accelerated away from the needle. The ions, as they move away, form a space charge region. This region behaves like a charge distribution and creates an electric field that superposes to the field created by the needle.

- **Neutralization region**

As the ions are repelled, the system becomes negatively charged and negatively charged particles need to be ejected by some means. These negative particles are electrons that meet the ion beam downstream to neutralize it in such a way that the plume expelled by the engine is neutral and the engine can also remain neutral. At the distance where these electrons meet the ion beam, the charge density becomes zero.

4.2 Relationship between the current and the voltage

The gas comes out through the needle tip into a vacuum where it is ionized such that the space charge only exists where there are gas molecules to be ionized. As mentioned earlier, the plasma region is negligible in all our investigations and we consider the space charge to form a cone from the needle tip. The space charge region can be pictured in spherical coordinates as shown on the figure below.

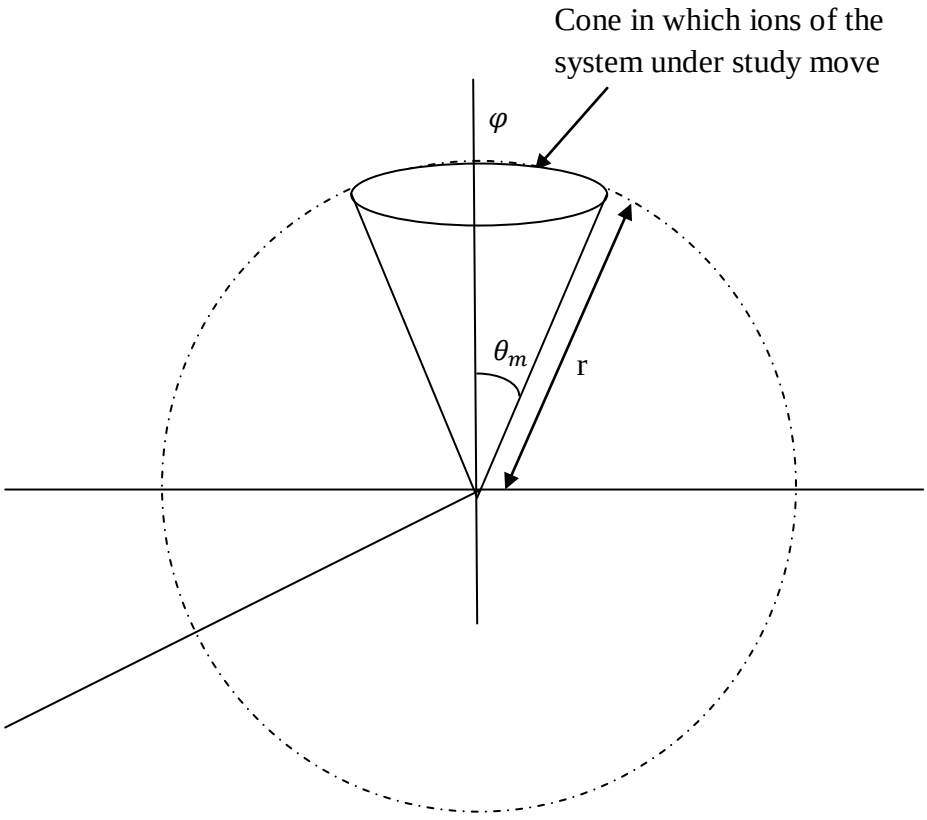


Figure 4.2: model of the plume in spherical coordinates

The spread angle is due to the repulsive forces between similarly charged particles and the neutral gas escaping into the vacuum from a small constriction, such as the needle hole.

4.2.1 Electric field of the system

In order to obtain the relationship between the voltage and the current, we follow Townsend's approach [23, 27], where he calculated the relationship for a co-axial cylindrical system. So we move from the Poisson equation in spherical coordinates by making the following assumptions:

1) The power into the plume has the effect of heating it in a direction away from the needle, increasing the average velocity
2) The needle tip produces a point charge like electric field
3) Potential at the needle tip is kept at zero. We consider the hypothetical voltage at the neutralization plane to be $-V$
4) The number of neutral particles is much larger than the ions and remains approximately constant with the current (but in reality, the number of neutrals in the plume = number of neutrals exiting –the number of ions)
5) The plume is cylindrically symmetric with a constant spread angle
6) Ions (not electrons) are assumed to be the only charge carriers in the ion region

7) Neutralization occurs at a fixed distance away from the needle tip, at the neutralization plane

8) The magnetic field is ignored because we are dealing here with a system with very small currents (of the order of a milliamp) [18].

9) The neutral gas density in the cone is assumed uniform. In reality, the gas density is higher in the center, with a density distribution given roughly by a sine function from 0 to π. The flow of the gas was also assumed to be laminar.

10) These assumptions are far from ideal but were used in order to capture the main physical effects, while remaining mathematically tractable. A lot of work can still be done to make the model more precise.

We need to solve the Poisson equation to obtain an expression for the effective electric field. Integration of the field will then yield a relationship between voltage and current. The Poisson equation in spherical coordinates is:

$$\frac{1}{r^2}\frac{\partial}{\partial r}\left(r^2\frac{\partial V}{\partial r}\right)+\frac{1}{r^2\sin\theta}\frac{\partial}{\partial\theta}\left(\sin\theta\frac{\partial V}{\partial\theta}\right)+\frac{1}{r^2\sin^2\theta}\frac{\partial^2 V}{\partial\varphi^2}=\frac{-\rho_{ion}}{\varepsilon_0}. \qquad (4.1)$$

Since the system has a symmetry under rotation along the direction φ, we ignore this variable, and we obtain

$$\frac{1}{r^2}\frac{\partial}{\partial r}\left(r^2\frac{\partial V}{\partial r}\right)+\frac{1}{r^2\sin\theta}\frac{\partial}{\partial\theta}\left(\sin\theta\frac{\partial V}{\partial\theta}\right)=\frac{-\rho_{ion}}{\varepsilon_0}\ . \qquad (4.2)$$

We will further calculate the space charge effects as if we had a spherically symmetric system: we do not calculate the electric field and space charge for the cone, but instead for a similar, but simpler system, namely that of a point charge in the center of an expanding gas cloud. The total current and neutral gas molecules in this system go through a cross-sectional area of $4\pi r^2$, the surface area of a sphere. To relate this to the system, we consider the current and neutrals going through the circular area of a cone cross section, and we ignore edge effects, similar to the space charge calculation of the Child-Langmuir law [28].

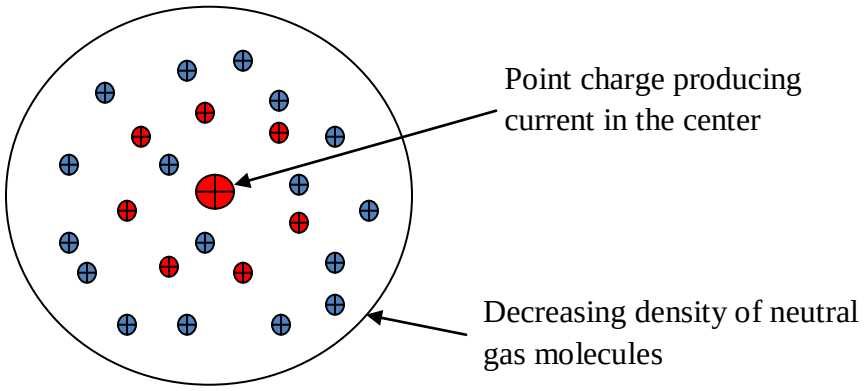


Figure 4.3: model of a point charge inside a sphere

The area of the spherical shell is given by

$$A = 4\pi r^2, \tag{4.3}$$

and the total current I emanates from the point charge in the center. This picture allows us to ignore angular effects, such that in the Poisson equation only the radial part needs to be considered. That is, equation (4.2) becomes

$$\frac{1}{r^2}\frac{\partial}{\partial r}\left(r^2\frac{\partial V}{\partial r}\right)=\frac{-\rho_{ion}}{\varepsilon_0}\ . \tag{4.4}$$

The general expression for a current is given by:

$$i=\rho(r).V(r).A(r), \tag{4.5}$$

where ρ is the charge density, V is the charge drift velocity and A is the area through which the ions move.

The total current going through a spherical surface centered on the charge at any distance is constant.

Since the plume is modeled by a cone and not the entire sphere, the area through which the ions move is

$$A(r)=2\pi r^2(1-cos\theta_m). \tag{4.6}$$

Further, for $\frac{E}{P}>10\ V.cm^{-1}.mmHg^{-1}$, which was the case in experiments, ($\sim 100\ V.cm^{-1}/\sim 10 mmHg^{-1}$) the drift velocity for an ion is proportional to $\sqrt{E/P}$ (the ratio of the electric field to the pressure is proportional to that of the electric field to the number density of molecules) [12, 20] and is given by:

$$V\cong\left(\frac{K}{2}\right)^{\frac{1}{4}}\left(\frac{e}{M}\right)^{\frac{1}{2}}(\lambda E)^{\frac{1}{2}}\ . \tag{4.7}$$

Here, K is the Fractional energy loss of an ion during a collision,e is the electron charge $1{,}6.10^{-19}C$, M is the mass of an ion≅ mass of a molecule (neutral) in kg, λ is the mean free path in meters and E the electric field generated by the needle, space charge corrected (V/m).

The neutral gas density at a distance r

In our case the density of the neutral gas molecules decreases with the distance travelled, implying that the mean-free-path increases. Next we know the mean free

path is inversely proportional to the number density (n) and the Scattering cross-section (σ). That is

$$\lambda = \frac{1}{n\sigma}\,.$$

Also the number density decreases outwards along the r −direction along the cone:

$$n(r) = \frac{number\ of\ neutrals}{volume\ at\ r} = \frac{number\ of\ neutrals}{A(r).dr} = \frac{number\ of\ neutrals}{2\pi r^2(1-cos\theta_m)dr}\,,$$

$$n(r) = n_0.\frac{1}{r^2}\,.$$

The outward flux of neutral gas molecules originates from the center of the spherical needle tip in this formulation. In practice it exits through the inner diameter. Yet this is a good approximation, as the center of the outward neutral flux and the center of the field lines are very close together. Hence,

$$\lambda = \frac{r^2}{n_0\sigma}\,. \qquad (4.8)$$

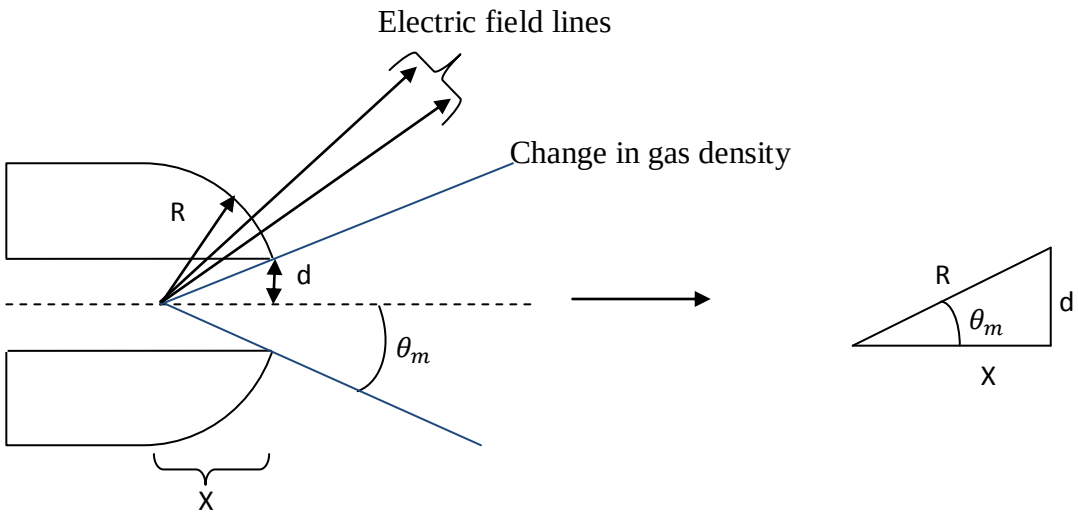


Figure 4.4: outward flux of neutral gas molecules

The density at the exit is the density of the emerging neutrals and the area is that of a section cut from a sphere of radius R. For details, see appendix A.

From $$n(r) = n_0 . \frac{1}{r^2}$$

we have

$$n(R) = n_0 . \frac{1}{R^2} = n_{exit} \ .$$

In order to determine the density at the exit, we consider the number of particles flowing through the cross-section of a tube of radius d. It is given by

$$n_{exit} = \frac{\dot{m}}{M \pi d^2 V_e},$$

where $\dot{m}$ is the mass flow rate, M is the molecular mass,d the inner diameter of the needle and V_e the gas exit velocity.

Now using a spherical shell rather than a flat circular area, we obtain

$$n_{exit} = \frac{\dot{m}}{M 2\pi V_e R^2 \left(1 - \sqrt{1 - \frac{d^2}{R^2}} \right)} \ .$$

Such that,

$$n_0 = \frac{\dot{m}}{M 2\pi V_e \left(1 - \sqrt{1 - \frac{d^2}{R^2}} \right)} \ . \qquad (4.9)$$

Substituting into equation (4.7) gives

$$V = \left(\frac{K}{2} \right)^{\frac{1}{4}} \left(\frac{e}{M} \right)^{\frac{1}{2}} (\lambda E)^{\frac{1}{2}} = \left(\frac{K}{2} \frac{e^2}{M^2} \frac{1}{n_0^2 \sigma^2} \right)^{\frac{1}{4}} . (r^2 E)^{\frac{1}{2}}$$

or

$$V(r) = C_0 \left(r^2 \frac{dV_r}{dr} \right)^{\frac{1}{2}}, \tag{4.10}$$

with

$$C_0 = \left(\frac{K}{2} \frac{e^2}{M^2} \frac{1}{n_0^2 \sigma^2} \right)^{\frac{1}{4}}. \tag{4.11}$$

The charge density

We chose $V = -C_0 \left(r^2 \frac{dV_r}{dr} \right)^{\frac{1}{2}}$ in order to make the sign of the following calculation consistent, that is so that the electric field magnitude remains real.

Putting this back into equation (4.5) will give the expression of the ion density as

$$\rho_e(r) = \frac{-I}{V(r).A(r)} = \frac{-I}{C_0 \left(r^2 \frac{dV_r}{dr} \right)^{\frac{1}{2}} . 4\pi r^2}. \tag{4.12}$$

This is the density of charge in the total spherical area. However, in our case, we only have charges in the conical area which is given by equation (4.6). Therefore the charge density there is given by

$$\rho_e(r) = \frac{-i}{C_0 \left(r^2 \frac{dV_r}{dr} \right)^{\frac{1}{2}} . 2\pi r^2 (1 - \cos\theta_m)}. \tag{4.13}$$

The electric field magnitude

Substitution of equation (4.13) into equation (4.4) gives the Poisson equation we are required to solve:

$$\frac{1}{r^2} \frac{d}{dr} \left(r^2 \frac{dV_r}{dr} \right) = \frac{i}{C_1 \left(r^2 \frac{dV_r}{dr} \right)^{\frac{1}{2}} r^2}, \tag{4.14}$$

with

$$C_1 = 2\pi\left(1-\cos\theta_m\right)\varepsilon_0 C_0 \ . \tag{4.15}$$

The solution of this differential equation is given by

$$\frac{dV_r}{dr} = \left(\frac{3i}{2C_1}\right)^{\frac{2}{3}} \frac{1}{r^2}\left(r + C_2\right)^{\frac{2}{3}} \ ; \tag{4.16}$$

see appendix B for details. Here C_2 is a constant to be determined. We follow the procedure of Townsend [27] and set the electric field at the needle tip to the smallest field at which breakdown occurs. Increasing the potential will lead primarily to an increase in current and a negligible increase in field at the needle tip.

$\left.\frac{dV_r}{dr}\right|_{r=R} = \frac{V_0}{R}$, which gives

$$C_2 = \frac{2C_1}{3i}\left(RV_0\right)^{\frac{3}{2}} - R \ . \tag{4.17}$$

Substituting into equation (4.16) gives the final expression for the space charge corrected radial electric field.

$$\frac{dV_r}{dr} = \left(\frac{3i}{2C_1}\right)^{\frac{2}{3}} \frac{1}{r^2}\left(r + \frac{2C_1}{3i}\left(RV_0\right)^{\frac{3}{2}} - R\right)^{\frac{2}{3}} . \tag{4.18}$$

This is the electric field created by both the point charge and the space charge region. Diagrams below are the graph of the corrected and the non-corrected electric field.

As $i \to 0$, it is seen that this field reduces to the correct limit, namely the point charge field.

In the graph shown in figure 3.3 it is seen that $\frac{\alpha}{P}$ (ionization efficiency) depends on $\frac{E}{P}$. Yet for the CorIon thruster, $\frac{E}{P} \sim \frac{E}{n}$ seems to be constant, since E and n both change as $\frac{1}{r^2}$. So, why should ionization occur at the needle tip, since $\frac{E}{P}$ suggests that it may do so at any point in the plume? If n were constant as in corona discharge in air, $\frac{E}{n}$ would be at a maximum at the tip, hence most ionization would occur there. Not so in the present case. The answer lies in the fact that the space charge distorts the field as can be seen from figure 4.5, increasing $\frac{E}{n}$ close to the needle and facilitating ionization there. The field is seen to increase close to the needle with increasing current, which is likely to be due to the increased positive ion density there. The field also increases further away from the needle for increased current, which is responsible for an electric breakdown throughout the entire plume, which has been observed experimentally.

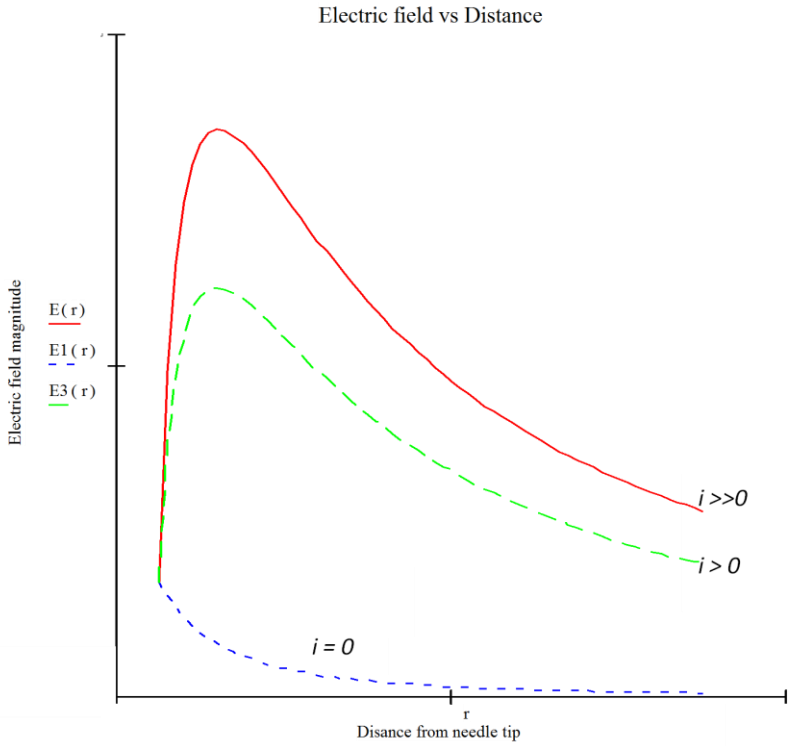


Figure 4.5: Electric field as a function of the distance from the needle tip for some values of the current

4.2.2 Relationship between the current and voltage

In order to obtain the relationship between the voltage and the current in the system, we integrate equation (4.21) from the needle-tip to the neutralization region.

For the case of a "cylinder-wire" configuration, Townsend took the current generating wire in the center of a cylinder as the ground ($V = 0$) where the voltage in the cylinder wall is increased to increase the current [27]. This leads to the boundary condition on the wire, namely that the field there must at least be sufficiently strong to start ionization of the gas.

To translate that to our situation, one needs to consider a spherical shell around the point charge whose potential is increased. Hence, the point charge should be viewed as "earthed" and the potential in the shell increased.

We must therefore include a potential surface (of a certain potential) in our calculations at distance D, the neutralization distance. The hope is that choosing the needle at $V = 0$ and a hypothetical plane with $V = -V$ will describe the same system as the needle at $V = V$ and the plane at $V = 0$

Therefore, we consider the integral of equation (4.16)

$$\int_R^D \frac{1}{r^2}\left(r + C_2\right)^{\frac{2}{3}} dr$$

$$= \frac{-a^2}{r} + \frac{1}{3b}\ln\left[\frac{\frac{a^2}{b^2} - \frac{2a}{b} + 1}{\frac{a^2}{b^2} + \frac{a}{b} + 1}\right] + \frac{\sqrt{12}}{3b}\arctan\left[\frac{2}{\sqrt{3}}\frac{a}{b} + \frac{1}{\sqrt{3}}\right]\Bigg|_R^D,$$

with $a = \left(r + C_2\right)^{\frac{1}{3}}$ and $b = C_2^{\frac{1}{3}}$, and by replacing a with its expression, obtain the potential difference given by

$$V = \left[\frac{-\left(D + C_2\right)^{\frac{2}{3}}}{D} + \frac{1}{3b}\ln\left[\frac{\frac{\left(D + C_2\right)^{\frac{2}{3}}}{b^2} - \frac{2\left(D + C_2\right)^{\frac{1}{3}}}{b} + 1}{\frac{\left(D + C_2\right)^{\frac{2}{3}}}{b^2} + \frac{\left(D + C_2\right)^{\frac{1}{3}}}{b} + 1}\right] + \frac{\sqrt{12}}{3b}\arctan\left[\frac{2}{\sqrt{3}}\frac{\left(D + C_2\right)^{\frac{1}{3}}}{b} + \frac{1}{\sqrt{3}}\right]\right.$$

$$\left. + \frac{\left(R + C_2\right)^{\frac{2}{3}}}{R} - \frac{1}{3b}\ln\left[\frac{\frac{\left(R + C_2\right)^{\frac{2}{3}}}{b^2} - \frac{2\left(R + C_2\right)^{\frac{1}{3}}}{b} + 1}{\frac{\left(R + C_2\right)^{\frac{2}{3}}}{b^2} + \frac{\left(R + C_2\right)^{\frac{1}{3}}}{b} + 1}\right] - \frac{\sqrt{12}}{3b}\arctan\left[\frac{2}{\sqrt{3}}\frac{\left(R + C_2\right)^{\frac{1}{3}}}{b} + \frac{1}{\sqrt{3}}\right]\right] \cdot \left(\frac{3i}{2C_1}\right)^{\frac{2}{3}}. \quad (4.19)$$

Which gives the voltage V of the shell at distance D as a function of the current. Also note that

$$\left(\frac{3i}{2C_1}\right)^{\frac{2}{3}} \cdot \frac{(R+C_2)^{\frac{2}{3}}}{R} = V_0.$$

The graphs below (figure 4.6 to figure 4.8) represent examples of the voltage, the power and the resistance of the new thruster as functions of the current for small current. They are meant to illustrate the basic behavior of equation (4.19)

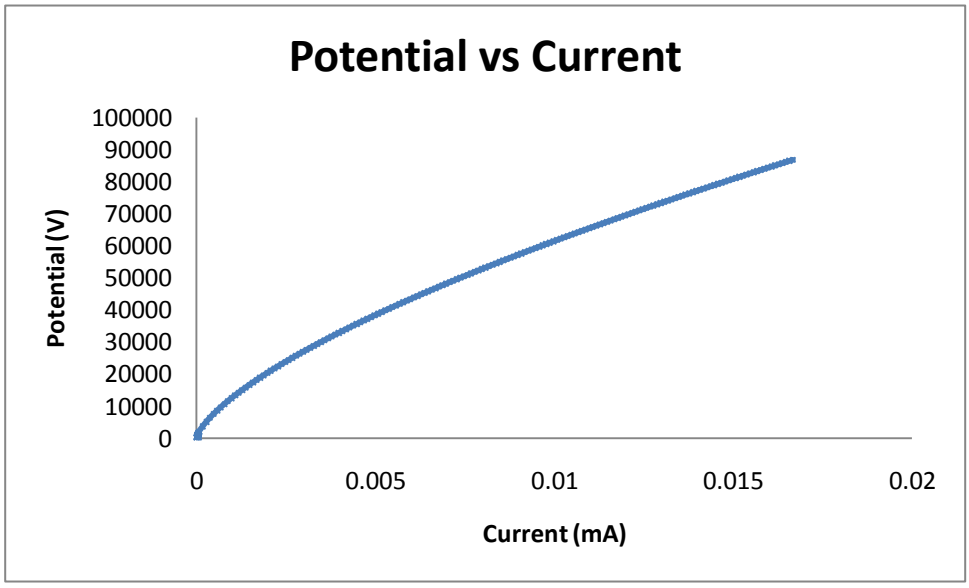


Figure 4.6: voltage as a function of the current

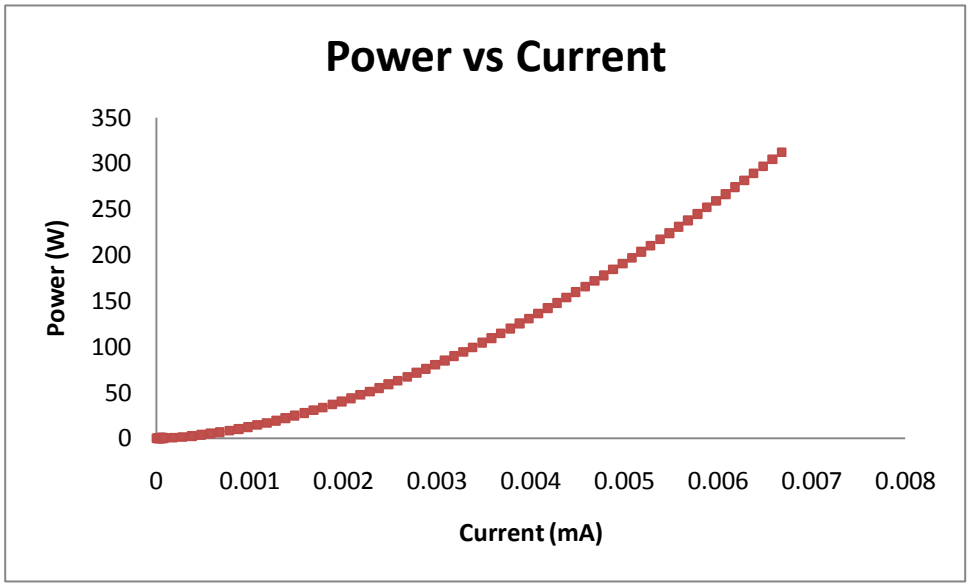


Figure 4.7: power as a function of the current

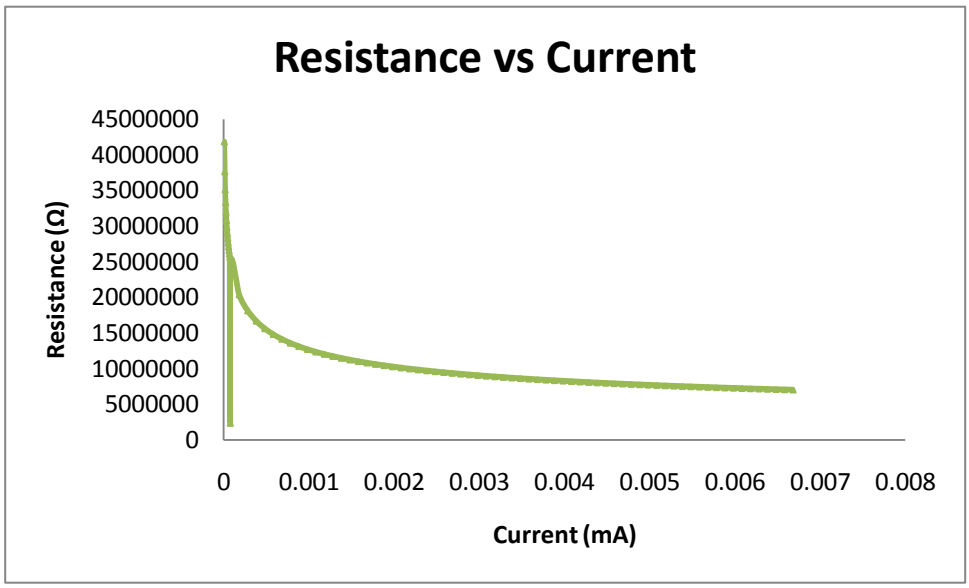


Figure 4.8: resistance as a function of the current

Chapter 5

Derivation of the Thrust

Here two different methods are used to find the thrust produced by the system. The first one is based on what we call the "vector heating" and the second is based on the principle of electrostatics.

5.1 Vector heating

We aim to estimate the thrust produced by the CorIon thruster using principles of molecular dynamics where we consider the thermal energy of the agitation of gas molecules in a container. From there we obtain the average velocity of the molecules when they escape the container through a small aperture where they have approximately the average thermal velocity. To include ionization effects we next consider the case where some molecules are ionized and accelerated by an electric field. From the kinetic theory of gases it is known that the mean velocity can be related to the mean temperature of the gas by [20]

$$\overline{V} = \sqrt{\frac{3kT}{M}} \ , \tag{5.1}$$

where k is the Boltzmann constant, T the absolute temperature of the gas and M its molecular mass.

Derivation of thrust equation

Molecules of a gas in a box are presumed to be in random motion with an average velocity which is a function of absolute temperature of the gas. If the gas molecules are escaping the box through an aperture, the mean velocity is approximately give by (5.1), and as illustrated in figure 5.1 below

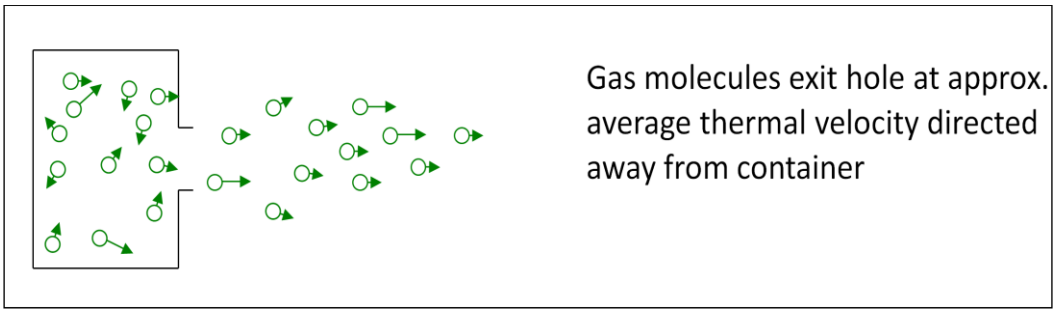


Figure 5.1: gas molecules escaping a box at approximately thermal velocity

The exiting molecules are subjected to an electric field created by a power supply with power P. As in positive corona, it is estimated that more than 95% of the electrical energy input is dissipated as heat into the neutral gas [29], where it can be concluded that a part of the electric power is used for the ionization of the gas and the biggest part is used to heat the gas, where figure 5.2 illustrates this

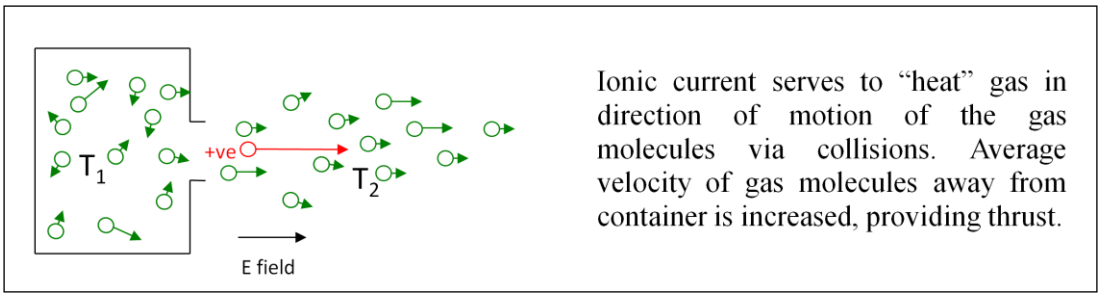


Figure 5.2: effect of the electrical energy on the molecules average velocity

Thus we can write

$$P = I' + H\,, \tag{5.2}$$

where I' is the ionization energy and H in given by the simple approximation:

$$H = Q = \dot{m}C\Delta T = \dot{m}C(T_2 - T_1). \tag{5.3}$$

Here $\dot{m}$ is the mass flow rate, C the heat capacity at constant pressure, T_1 the temperature of the cold exhaust and T_2 the final temperature.

Though the heat capacity being at constant pressure is assumed this needs to be examined much more closely: neither the pressure nor the volume of the gas remains constant in this system. However, since most heating occurs in a small region close to the needle, we suggest that the heat capacity does not vary much.

As such, equation (5.2) and (5.3) give us

$$P - I' = \dot{m}C\left(T_2 - T_1\right)\,,$$

or

$$\frac{P - I'}{\dot{m}C} + T_1 = T_2\ . \tag{5.4}$$

The thrust equation can be written as

$$F = \dot{m}\Delta V = \dot{m}\left(\overline{V_2} - \overline{V_1}\right)\,, \tag{5.5}$$

and using equations (5.4) and (5.5), the final expression of the thrust is given by

$$F = \dot{m}\sqrt{\frac{3K}{M}}\left[\left(\frac{P - I'}{\dot{m}C} + T_1\right)^{1/2} - T_1^{1/2}\right]\ . \tag{5.6}$$

This expression suggests that the thrust is reduced with increasing molecular mass and increased heat capacity, while increasing with mass flow rate.

Note that beam spreading given by equation (2.12) is ignored in all these calculations, as well as cold thrust (thrust arising from the un-ionized propellant)

5.2 The Electrostatic method

We follow the basic procedure of Jack Wilson et al. [30] to calculate thrust using electrostatic interactions. To derive the thrust equation, we consider the following system (see figure 5.4)

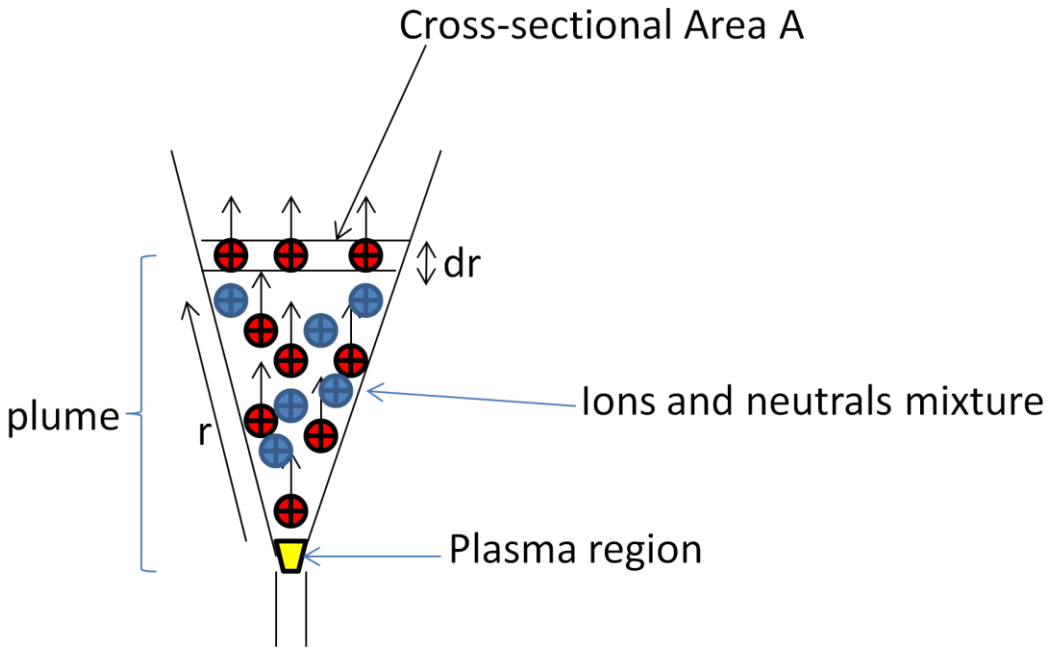


Figure 5.3: model of the plume for the thrust

We consider the force on a charge as given by

$$F = qE.$$

As such the total force on n charges is

$$F_T = nqE. \tag{5.8}$$

Next, using the definition for the current (refer to figure 5.4):

$$i = \rho(r).\mathrm{V}(r).A(r), \tag{5.9}$$

where $\frac{number\ of\ charges}{volume} = \frac{nq}{A(r).dr}$,

q is the elementary charge,$A(r)$ the cross-sectional area at a distance r from the needle tip $\mathrm{V}(r)$ the ion drift velocity at a distance r from the needle tip.

Which means

$$i = \frac{nq}{dr}\mathrm{V}(r).$$

This is the current in a volume element of the expanding plume. Recalling the expression for the drift velocity from the last chapter (equation (4.10)), we obtain

$$i = \frac{nq}{dr} C_0.r.\sqrt{E}$$

$$\Rightarrow nq = \frac{idr}{C_0.r.\sqrt{E}}.$$

Hence the force acting on an infinitesimal sliver of the plume is

$$dF_T = \frac{iEdr}{C_0.r.\sqrt{E}}$$

$$= \frac{i}{C_0}.\frac{\sqrt{E}}{r}.dr$$

$$= \frac{i}{C_0} \cdot \frac{\left[\left(\frac{3i}{2C_1} \right)^{\frac{2}{3}} \cdot \frac{1}{r^2} \left(r + C_2 \right)^{\frac{2}{3}} \right]^{\frac{1}{2}}}{r} .dr$$

$$= \frac{i}{C_0} \cdot \left(\frac{3i}{2C_1} \right)^{\frac{1}{3}} \frac{1}{r^2} \left(r + C_2 \right)^{\frac{1}{3}} .dr$$

$$F_T = \frac{i}{C_0} \cdot \left(\frac{3i}{2C_1} \right)^{\frac{1}{3}} \int_R^D \frac{1}{r^2} \left(r + C_2 \right)^{\frac{1}{3}} .dr.$$

Where C_0 is defined by equation (4.11), C_1 by (4.15), C_2 by (4.17), R the needle outer radius and D the neutralization distance.

The integral

$$\int_R^D \frac{1}{r^2} \left(r + C_2 \right)^{\frac{1}{3}} .dr \; = \frac{-a}{r} + \frac{1}{6b^2} \ln \left[\frac{\frac{a^2}{b^2} - \frac{2a}{b} + 1}{\frac{a^2}{b^2} + \frac{a}{b} + 1} \right] + \frac{\sqrt{12}}{6b^2} \arctan \left[\frac{2}{\sqrt{3}} \frac{a}{b} + \frac{1}{\sqrt{3}} \right] \Bigg|_R^D .$$

Such that the total force, which is also the total thrust produced by the thruster, is given by

$$F_T = \frac{i}{C_0} \cdot \left(\frac{3i}{2C_1} \right)^{\frac{1}{3}} \left[\frac{-a}{r} + \frac{1}{6b^2} \ln \left[\frac{\frac{a^2}{b^2} - \frac{2a}{b} + 1}{\frac{a^2}{b^2} + \frac{a}{b} + 1} \right] + \frac{\sqrt{12}}{6b^2} \arctan \left[\frac{2}{\sqrt{3}} \frac{a}{b} + \frac{1}{\sqrt{3}} \right] \Bigg|_R^D \right],$$

with $a=\left(r+C_2\right)^{\frac{1}{3}}$ and $b=C_2^{\frac{1}{3}}$. Replacing a, we obtain

$$F_T=\frac{i}{C_0}\cdot\left(\frac{3i}{2C_1}\right)^{\frac{1}{3}}\left[\frac{-\left(D+C_2\right)^{\frac{1}{3}}}{D}+\frac{1}{6b^2}\ln\left[\frac{\frac{\left(D+C_2\right)^{\frac{2}{3}}}{b^2}-\frac{2\left(D+C_2\right)^{\frac{1}{3}}}{b}+1}{\frac{\left(D+C_2\right)^{\frac{2}{3}}}{b^2}+\frac{\left(D+C_2\right)^{\frac{1}{3}}}{b}+1}\right]+\frac{\sqrt{12}}{6b^2}\arctan\left[\frac{2}{\sqrt{3}}\frac{\left(D+C_2\right)^{\frac{1}{3}}}{b}+\frac{1}{\sqrt{3}}\right]\right]$$

$$-\frac{i}{C_0}\cdot\left(\frac{3i}{2C_1}\right)^{\frac{1}{3}}\left[\frac{-\left(R+C_2\right)^{\frac{1}{3}}}{R}+\frac{1}{6b^2}\ln\left[\frac{\frac{\left(R+C_2\right)^{\frac{2}{3}}}{b^2}-\frac{2\left(R+C_2\right)^{\frac{1}{3}}}{b}+1}{\frac{\left(R+C_2\right)^{\frac{2}{3}}}{b^2}+\frac{\left(R+C_2\right)^{\frac{1}{3}}}{b}+1}\right]+\frac{\sqrt{12}}{6b^2}\arctan\left[\frac{2}{\sqrt{3}}\frac{\left(R+C_2\right)^{\frac{1}{3}}}{b}+\frac{1}{\sqrt{3}}\right]\right]. \quad (5.10)$$

Again, the beam spreading is ignored and the cold thrust must be subtracted from the final thrust measurement.

Chapter 6

Prior Experimental Results

6.1 Experimental objectives

We now aim to test our mathematical model using some experimental data of the proposed thruster. Experimental data presented in this section were obtained by Adiv Maimon at the University of Cape Town as we could not perform the experiment within the School of Physics of the University of the Witwatersrand due to the poor quality of the vacuum available.

From the previous sections it can be seen that the performance parameters of the thruster are related to the following primary parameters, which can be easily measured.

- Mass flow rate
- Thrust
- Voltage across the thruster
- Current flowing through the thruster

6.2 Experimental equipment and setup

A thruster was built and clamped on a pendulum stand. A Hall-effect sensor was used to measure the thrust. The thruster and the sensor are presented on figure 6.1 below.

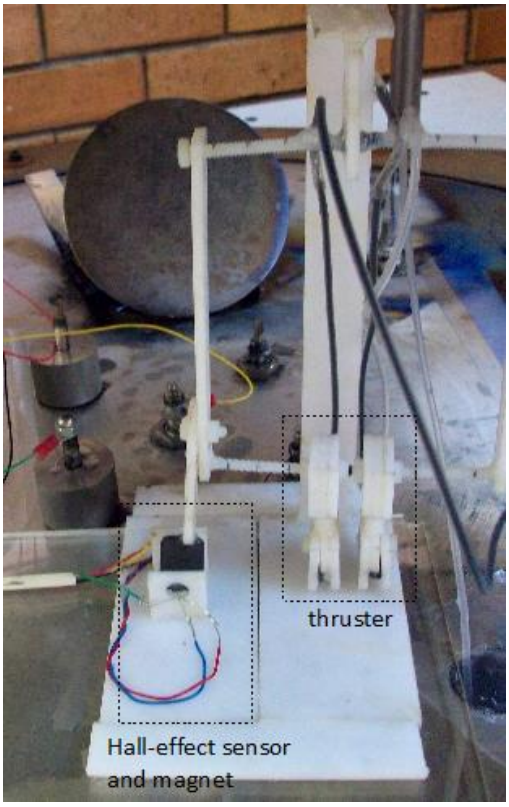


Figure 6.1: final sensor and thruster setup [25]

The power supply was made of:

- A Variac, to vary the input voltage
- A high voltage (9kV) transformer
- A full-bridge rectifier
- Some smoothing capacitors
- A circuit to allow for measuring the high voltage and current without damaging any equipment

All these equipments and their connections are shown in the figure 6.2.

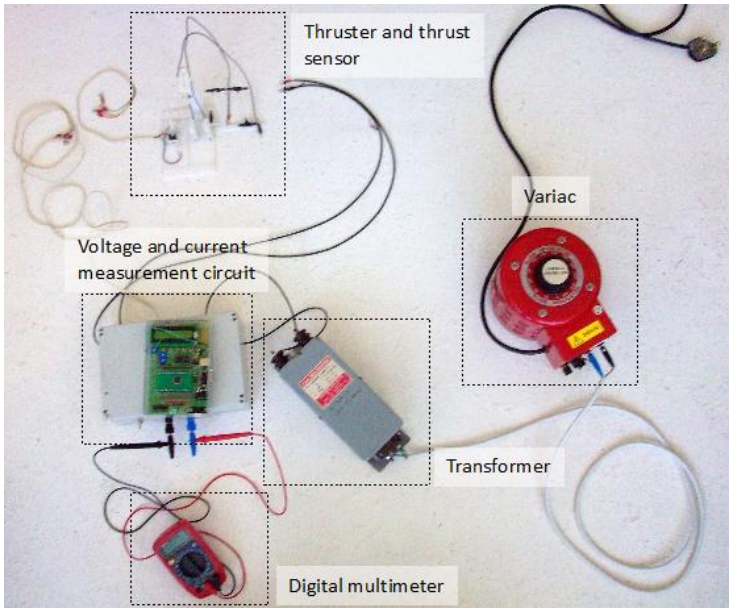


Figure 6.2: Equipment layout

Other important equipment includes a vacuum chamber, a vacuum pump to create a space-like environment, and a power supply to provide the necessary voltage for corona to take place. Figure 6.3 shows the vacuum chamber and equipment setup.



Figure 6.3: Vacuum chamber and equipment

After the calibration of the Hall-effect sensor and the pendulum, safety precautions were taken and the following two experiments performed:

6.3 Experiment 1

6.3.1 Experiment

This experiment aimed to test the effect of different needle types on the performance of the thruster. Three needles were used:

- A stainless steel surgical needle with a 500 micron inner diameter and a fairly flat tip [needle 1]

- A stainless steel needle with a 40 micron inner diameter and a very sharp tip [needle 2]
- A copper needle of 10 micron inner diameter and very sharp tip [needle 3]

Thrust and current were measured for a series of voltage inputs, the voltage at which the plume is observed was recorded and pictures taken. This was done for all the needles for a similar mass flow rate.

6.3.2 Presentation of results

Graphs on figure 6.4 to 6.6 show the measured quantities in graphical format. For more information about this experiment, see [25].

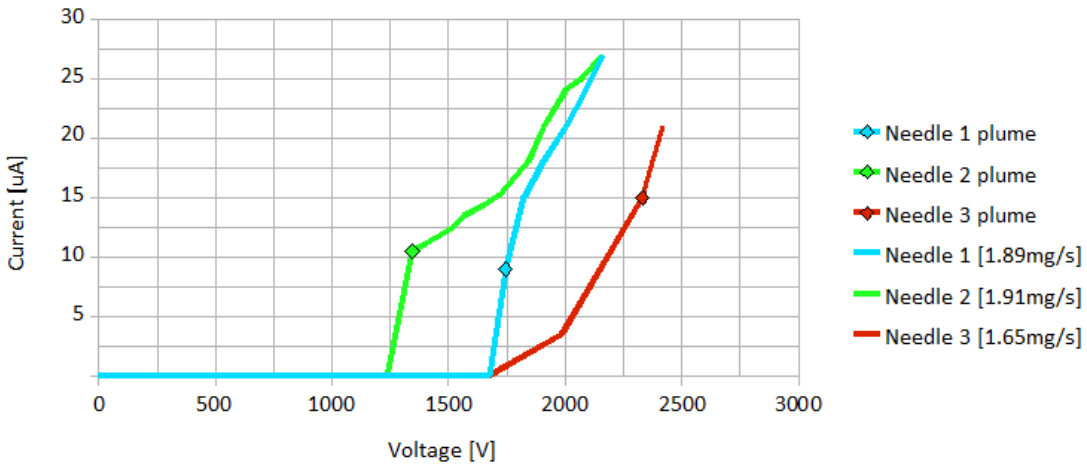


Figure 6.4: Measurements of current for experiment 1 [25]

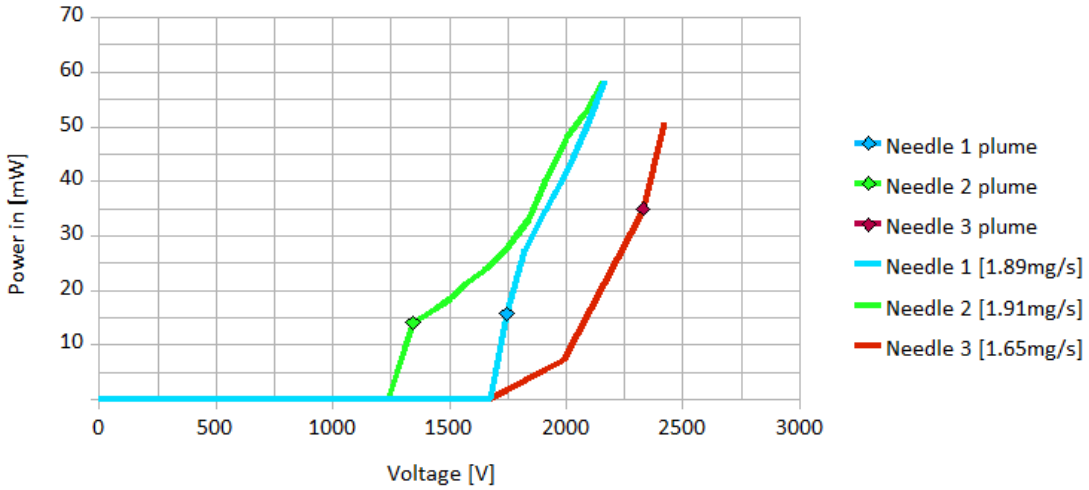


Figure 6.5: Electrical power usage for experiment 1 [25]

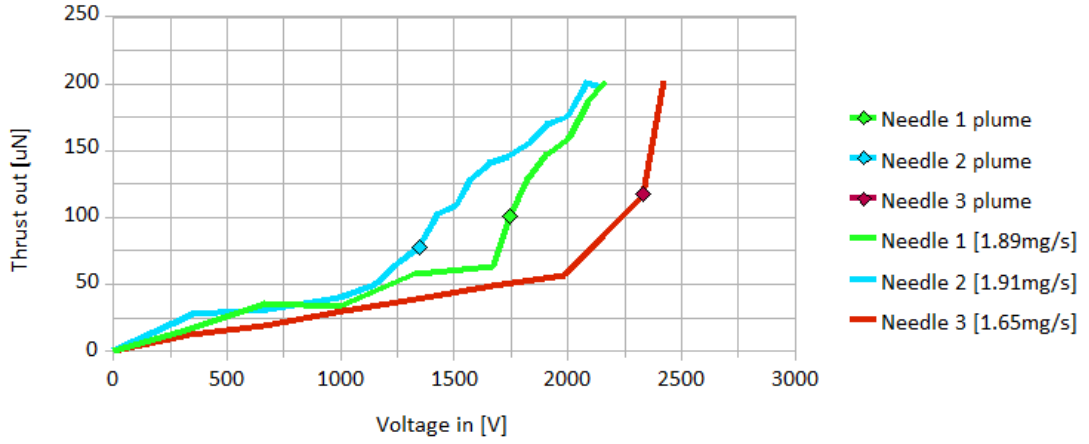


Figure 6.6: Measurements of thrust for experiment 1 [25]

6.4 Experiment 2

6.4.1 Experiment

This experiment aimed to record the effects of different mass flow rate for the same needle.

Again, thrust and current were measured for a series of voltage inputs, the voltage at which the plume is observed was recorded and pictures taken for one needle but at different mass flow rates.

6.4.2 Presentation of results

Graphs in figure 6.7 to 6.9 show the measured quantities in graphical format.

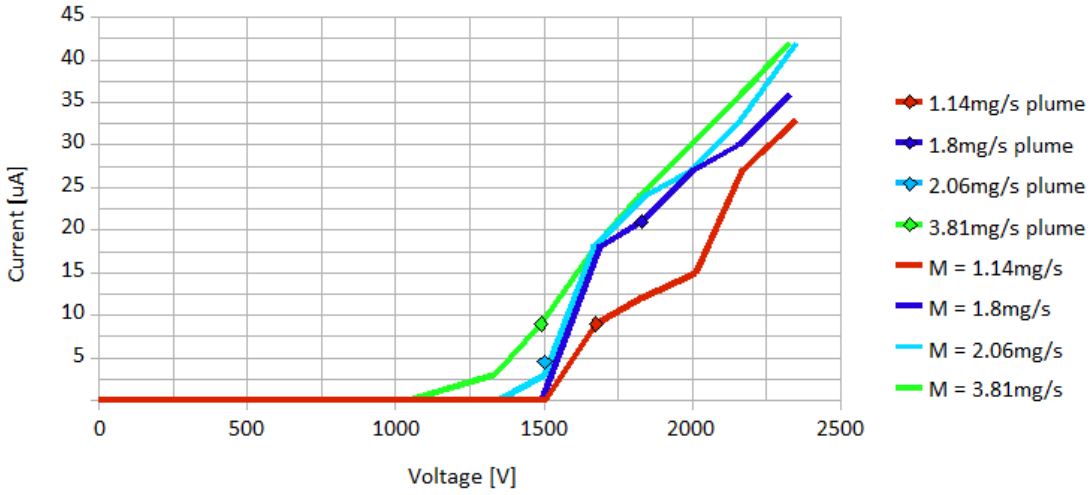


Figure 6.7: Measurements of current for experiment 2 [25]

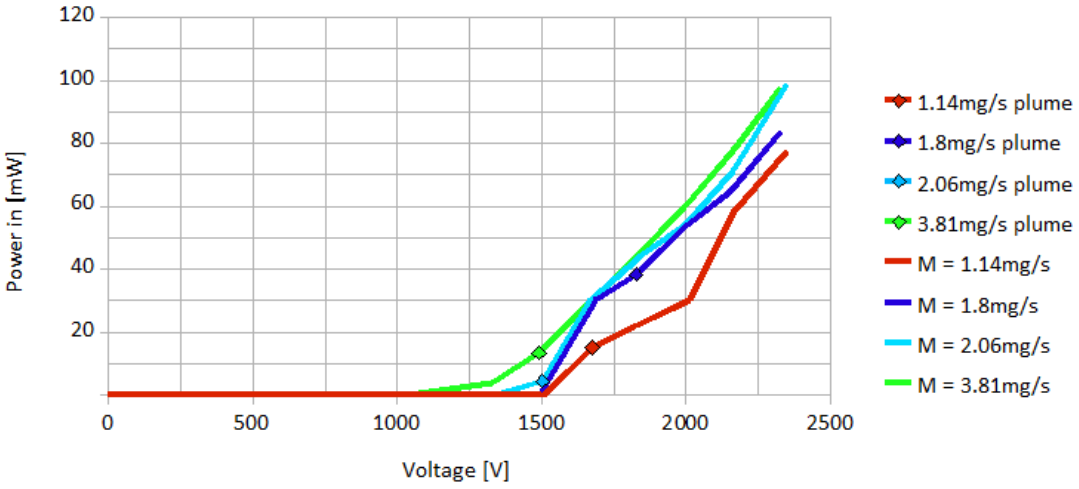


Figure 6.8: Electrical power usage for experiment 2 [25]

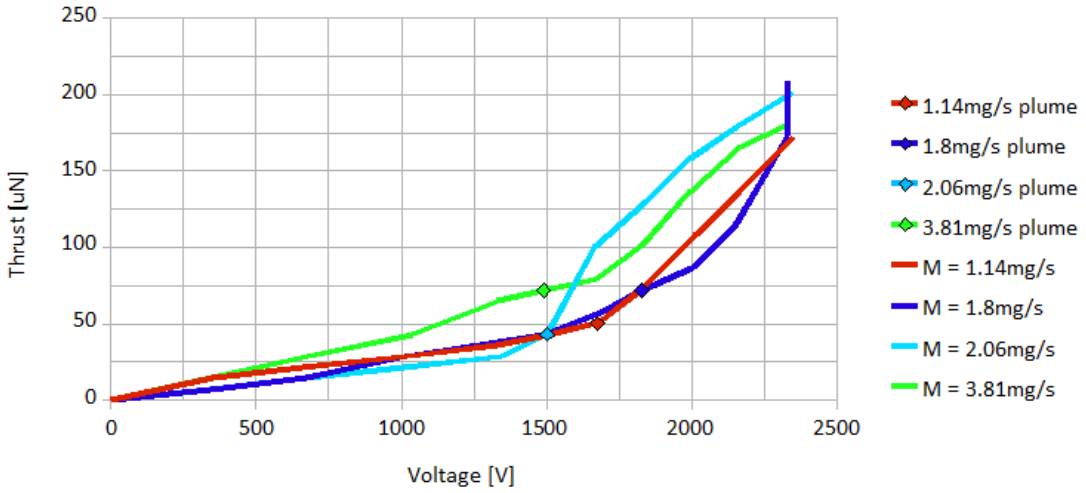


Figure 6.9: Measurements of thrust for experiment 2 [25]

From this experiment the conclusion drawn was that the stainless steel needle with a 40 micron inner diameter and a very sharp tip gave the highest thrust for medium power consumption. The results from this needle will be used in the next chapter for comparison with theory. Figure 6.10 below shows one of the plumes observed during the experiment

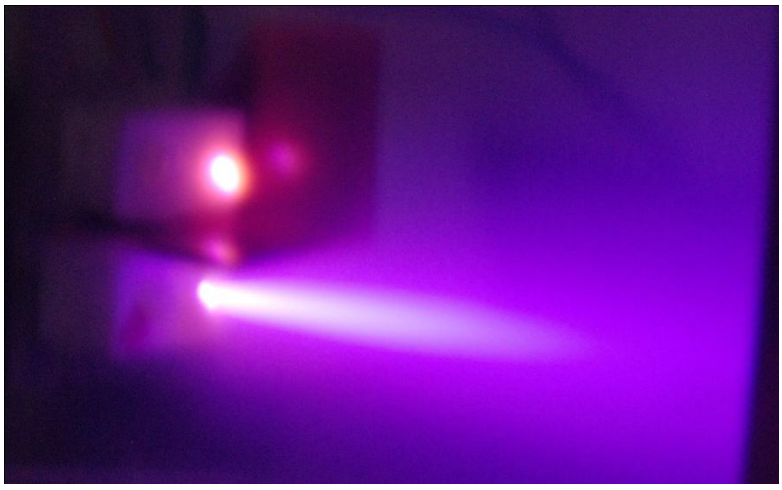


Figure 6.10: plume of the CorIon thruster in operation

Chapter 7

Comparison of Theory and Experiment

In this section, we do a critical investigation of the proposed thruster by comparing the theoretical results with the experimental data.

From the experiment described in chapter 6 we obtain the following table 7.1 for the stainless steel needle with a 40 micron inner diameter and a very sharp tip (Needle 2) with a mass flow rate of $1.91\ mg/s$. This needle seems to have given better results than the others. Here, the onset potential is taken as the part of the voltage that goes into the ionization of the propellant. Note that as [25] does not give any error on his measurements, we assume conservative errors by inspection.

Table 7.1: estimation of experimental data (onset voltage$= 1250\ \pm 50\ V$)

Voltage (V) ∓ 50 V	Current(μA) $\mp 2\ \mu A$	Input Power (W)	$V - V_0$ ∓ 50 V	Thrust (μN) $\mp 20 \mu N$	Thrusting Power (W)
1300	5	0.007 ∓ 0.003	50	15	0.00025
1350	10	0.014 ∓ 0.003	100	40	0.001
1750	15	0.027 ∓ 0.004	500	115	0.0075
1850	20	0.037 ∓ 0.005	600	135	0.012
2100	25	0.053 ∓ 0.005	850	165	0.0213

In tables 7.2 and 7.3, we give the physical parameters of the needle as well as those of the gas. Note that the gas used for this investigation was Nitrogen.

Table 7.2 Physical dimensions

PHYSICAL PARAMETERS	DIMENSION (m)
Needle outer radius	0.00005
Needle inner radius	0.00004
Neutralization distance	0.15

Table 7.3: Gas parameters

Molecular mass	$4.6x10^{-26}$ kg
Exit velocity	40 m/s
Temperature	1.7 K
Heat capacity (Nitrogen)	1040 J/kg.K
Spread angle	1.5 rad
Mass flow rate	1.91 mg/s

Using these parameters, we obtain our theoretical values of the voltage, power and thrust, as presented in table 7.4 for a range of currents

Table 7.4: theoretical parameters of the thruster

Current (μA)	Potential (V)	Power (W)	Vector heating thrust (μN)	Electrostatic thrust (μN)
5	209.12	0.0011	10.78	3.14
10	376.20	0.0038	33.89	6.53
15	526.42	0.0079	61.72	10.12
20	665.89	0.013	91.27	13.88
25	797.51	0.020	121.13	17.78

From the tables above, we plot on the same graph the experimental data and theoretical predictions of the thruster for the same range of current flowing through the system.

7.1 Voltage Vs Current comparison

In the figure 7.1 below, it can be seen that there is a reasonable agreement between the theory and the experiment even though there are some discrepancies that we cannot explain for the lower current values.

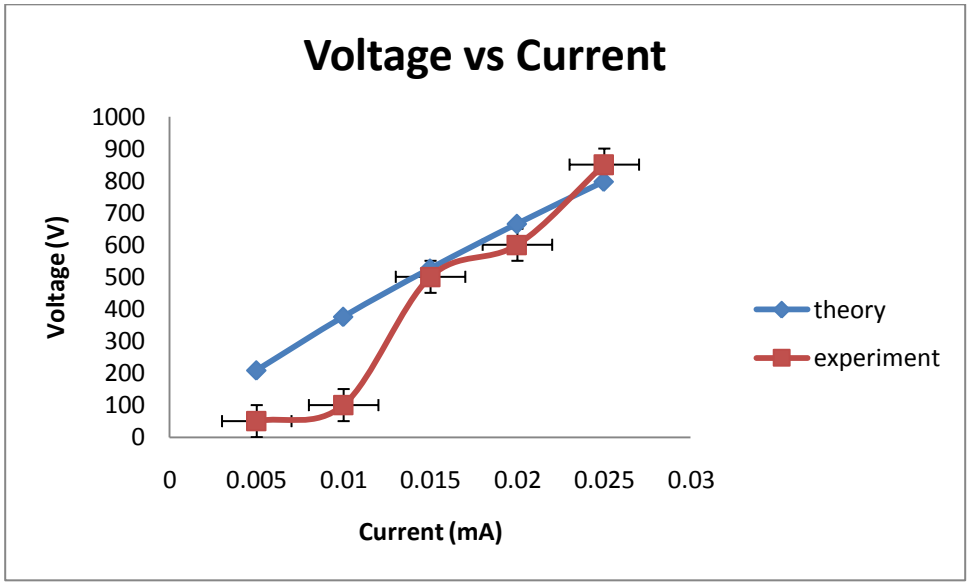


Figure 7.1: comparison of theoretical and experimental voltage

7.2 Power Vs Current comparison

In figure 7.2 the curve labeled “experimental power (ionization + thrusting)” gives the total power consumed by the thruster. Subtraction of the ionization power results in the curve “experimental thrusting power” which is compared to the theoretical prediction, displayed as “theory”. It can be seen that there is again good agreement between the two curves. The onset voltage gives an indication of the power needed to ionize the propellant, where the ionization power is given by

$$P_{ion} = V_0 . i \ .$$

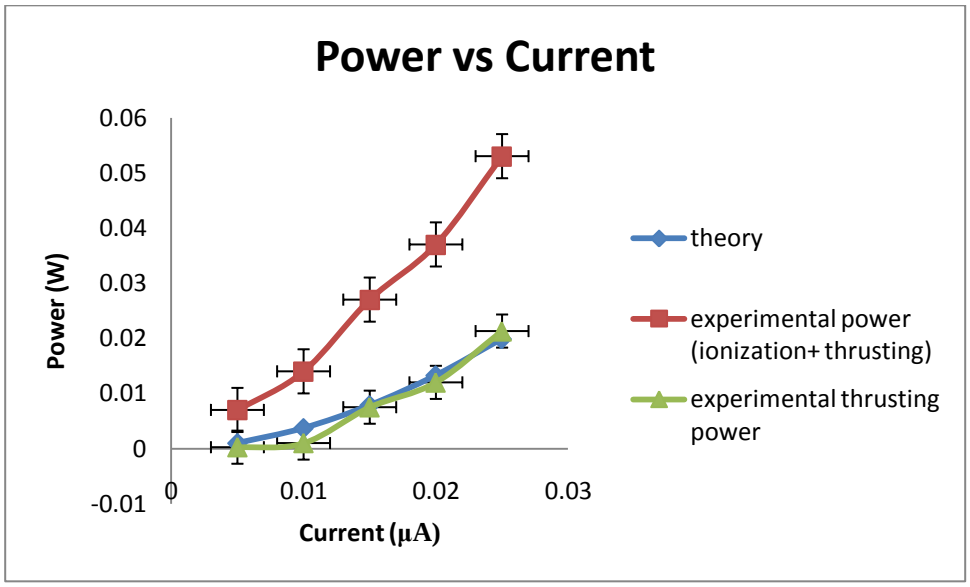


Figure 7.2: comparison of theoretical and experimental power

7.3 Thrust comparison

In figure 7.3, the "vector heating" formalism gives a reasonable description of the thrust when $T_1 = 1.7\ K$ (40 m/s exit velocity). It performs better in describing the thrust than the electrostatic formalism.

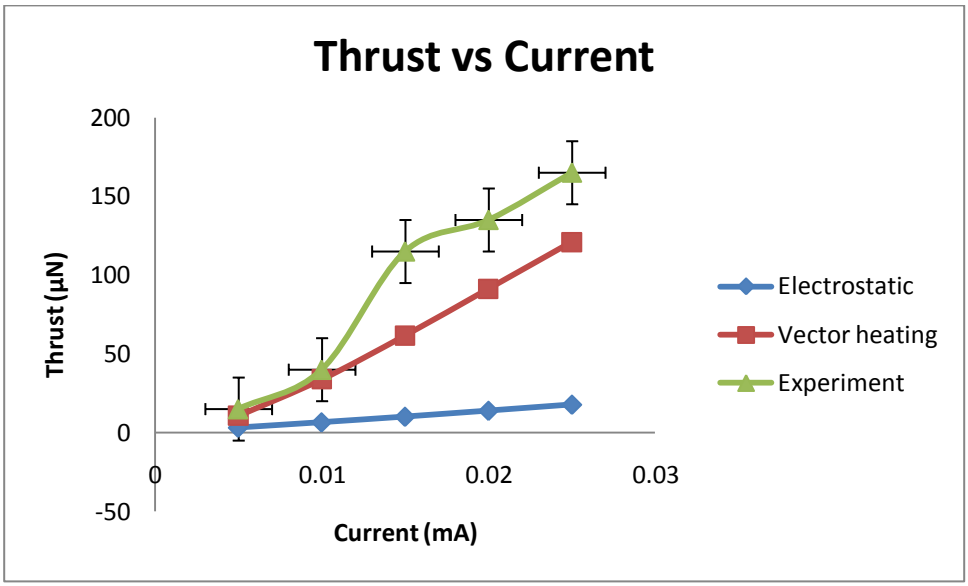


Figure 7.3: comparison of theoretical and experimental thrust

Note that the experiment yields more (about 10 times) thrust than expected from the electrostatic prediction.

One possibility is that experimental errors are larger than estimated, which may be possible due to the sensitivity of the experiment.

Electrons back streaming also contribute to the experimental thrust as electrons are accelerated, collide with gas molecules, and are reaccelerated. However, due to their small mass, this contribution is likely to be small.

Another possibility is that the plume could be pushing against gas molecules present in the chamber, creating a pressure difference that might also contribute to the thrust.

More exotic effects such as plasma phenomena are not considered in the theoretical study of the thruster. Electrostatic interactions within the equipment are unlikely to make a difference, since forces were examined before Corona and design features like the bipolar thruster are meant to minimize these forces.

It is clear therefore that the electrostatic prediction underestimates the thrust. The reason for this is not entirely clear at this stage but it may be due to the electrostatic prediction being more difficult accounting for all the physical phenomena occurring in the system. More investigation is needed before a good conclusion can be drawn.

One may conclude that since the "vector heating" gives a better description, while not referring to the electrostatic nature of the thruster, some part of the thrust is likely to be of a different origin than electrostatic.

7.4 Further comparison: Effects of the mass flow rate

Effects of the mass flow rate on the voltage

Theory predicts higher voltage for higher flow rate at the same current (formula (4.9) to (4.19)). The table 7.5 below gives us the values of the potential difference for different flow rates.

Table 7.5: change in voltage at different flow rate at the same current

Current (mA)	Voltage $\pm 50\ V$ ($\dot{m}$=1.8mg/s)	Voltage $\pm 50\ V$ ($\dot{m}$=2.06mg/s)	Voltage $\pm 50\ V$ ($\dot{m}$=3.81mg/s)
0.005	50	150	200
0.01	100	250	400
0.015	200	350	525
0.02	300	400	600
0.025	400	525	750

As can be seen in figure 7.4, the experiment is in qualitative agreement with theory.

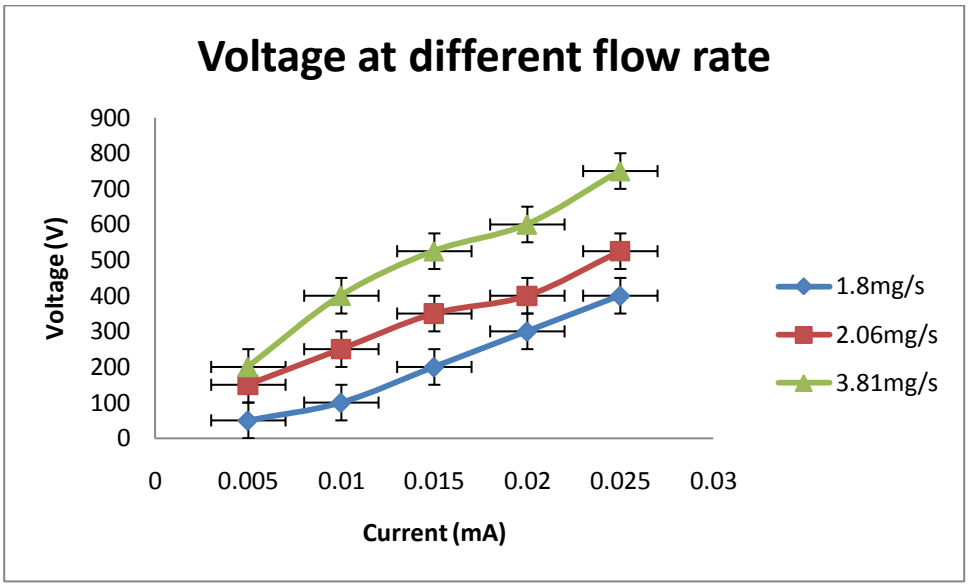


Figure 7.4: change of the potential difference with the flow rate

Any vertical line for any constant current predicts a voltage increased for increasing flow rate. This qualitative trend is visible in figure 7.4

Chapter 8

Conclusion and Outlook

8.1 Conclusion

In this dissertation a novel type of electrostatic thruster was introduced. The Corona Ionization (CorIon) Space Propulsion system is an electrostatic propulsion system intended for use on satellites and for deep space probes. Its advantages include it having a small mass, low complexity and small cost.

After showing that the incomplete ionization of the propellant can be advantageous for a thruster, we gave a first approximation mathematical model describing the electric field, the potential difference and the thrust produced. Considering the needle tip as a point charge and the exhaust plume to be cylindrically symmetric with a constant spread angle, we obtained an expression for the electric field and the potential difference of the system by solving the Poisson equation in spherical coordinates. Note that the graphs plotted in chapter 7 showed that a reasonable agreement with experimental results exists.

We then derived the thrust using conservation of energy (vector heating) and a more popular method (electrostatic). From the graph plotted, figure 7.3, we can conclude that between the two methods the "vector heating" is the one which has a more realistic prediction of the thrust produced by the system. The experimental thrust is almost ten times that predicted by the electrostatic model. For now, all we can say is that it is encouraging that we obtain more thrust than predicted. Some possible explanations were proposed: experimental errors, electrons back streaming,

plasma effects; also, that the thrust may have an origin different from electrostatic, etc.

Also note that in this entire dissertation, the magnetic field is ignored as we have a very small current flowing in the system (of the order of 10^{-3}A) [12] and furthermore the magnetic field would act to diminish the spread of the plume.

8.2 Outlook

This was a first attempt at describing this new system and many approximations were made. For a more realistic model, the approximations made in section 4.2.1 need to be examined more closely. Nevertheless, we were able to show reasonable agreement.

We introduced the Corona Ionization space propulsion system and gave a first approximation mathematical model of the system which we compared experimental data. For this new system to be competitive with existing technology, the following issues need to be addressed:

From the study of the corona, we know that a part of the energy input into the system excites atoms rather than ionizing them. We need a model that takes into account this part of the energy.

In solving the Poisson equation we made numerous approximations, as it was not easy to solve accurately. The next step here could be to make an entirely computational modeling of the system that will use more realistic parameters.

In the experiment we obtained more thrust than expected and that the thrust increased with increasing flow rate. We also had an anomaly that we thought was due to the change in the flow regime. We need to investigate the influence of the flow regime on the thruster parameters, in order to obtain a more realistic idea of how the neutral gas exits the needle into the vacuum.

Overall, our new thruster produces thrust in accordance with the theoretical predictions. Since the system is new and not well understood, much more work still needs to be done. The model also seems to be in very good agreement with the experiments except that the thrust is underestimated by the model. More experiments must be performed in space-like environments and more computations done before this new thruster can be accepted or rejected

Appendix A

Number density

The number density is given by

$$n(r) = \frac{number\ of\ neutrals}{volume\ at\ r} = \frac{number\ of\ neutrals}{A(r).dr} = \frac{number\ of\ neutrals}{2\pi r^2(1-cos\theta_m)dr},$$

where the number density decreases along the r −direction of the cone:

$$n = n_0.\frac{1}{r^2}\,.$$

If we consider a tube of radius d , the number of particles flowing through the cross section of the tube per second is given by

$$n_0 = \frac{\frac{\dot{m}}{M}}{\pi V_e d^2} = \frac{\dot{m}}{M\pi d^2 V_e}\ .$$

The diagram in figure A.1 describes this in more detail

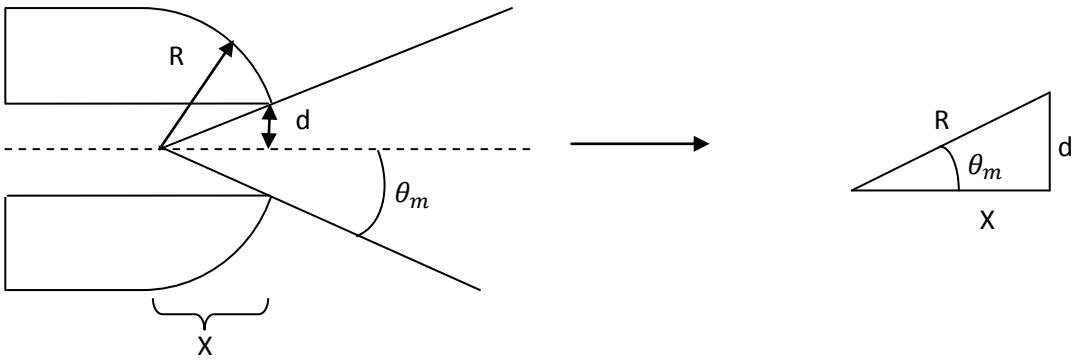


Figure A.1: Schematic of a gas exiting a tube of radius d

From this figure, one can see that

$$\cos\theta_m = \frac{X}{R} = \sqrt{\frac{R^2 - d^2}{R^2}} = \sqrt{1 - \frac{d^2}{R^2}}.$$

The outward flux of neutrals originates from the center of the spherical needle tip in this formulation. In practice, it exits through the inner diameter. Yet this is a good approximation, since the center of the outward neutral flux and the center of the field lines are very close together.

The density at the exit is the density of the emerging neutrals, and the area is that of a cut section from a sphere of radius R.

From $$n(r) = n_0 . \frac{1}{r^2}$$

we have

$$n(R) = n_0 . \frac{1}{R^2} = n_{exit}.$$

In order to determine the density at the exit, we consider the number of particles flowing through the cross-section of a tube of radius d. It is given by

$$n_{exit} = \frac{\dot{m}}{M \pi d^2 V_e}.$$

Using a spherical shell rather than a flat circular area, we obtain

$$n_{exit} = \frac{\dot{m}}{M 2\pi V_e R^2 \left(1 - \sqrt{1 - \frac{d^2}{R^2}}\right)},$$

such that

$$n_0 = \frac{\dot{m}}{M 2\pi V_e \left(1 - \sqrt{1 - \frac{d^2}{R^2}}\right)} \quad \text{and} \quad n = \frac{\dot{m}}{M 2\pi V_e \left(1 - \sqrt{1 - \frac{d^2}{R^2}}\right)} \frac{1}{r^2}.$$

Appendix B

Calculation of the Electric Field

Moving from

$$\frac{1}{r^2}\frac{d}{dr}\left(r^2\frac{dV_r}{dr}\right)=\frac{i}{4\pi\varepsilon_0 C_0\left(r^2\frac{dV_r}{dr}\right)^{\frac{1}{2}}r^2}$$

$$\frac{1}{r^2}\frac{d}{dr}\left(r^2\frac{dV_r}{dr}\right)=\frac{i}{C_1\left(r^2\frac{dV_r}{dr}\right)^{\frac{1}{2}}r^2}\ ,$$

where

$$C_1=2\pi\left(1-\cos\theta_m\right)\varepsilon_0 C_0\ .$$

Substituting $u=r^2\frac{dV_r}{dr}$ yields

$$\frac{du}{dr}=\frac{i}{C_1}\frac{1}{u^{1/2}}$$

$$\Rightarrow u^{1/2}du=\frac{i}{C_1}dr$$

$$\Rightarrow \int u^{1/2}du=\frac{i}{C_1}\int dr$$

$$\Rightarrow \frac{2}{3}u^{3/2} = \frac{i}{C_1}\left(r + C_2\right)$$

$$\Rightarrow u^{3/2} = \frac{3i}{2C_1}\left(r + C_2\right).$$

Here C_2 is a constant to be determined, therefore

$$\Rightarrow u = \left(\frac{3i}{2C_1}\right)^{\frac{2}{3}}\left(r + C_2\right)^{\frac{2}{3}}$$

$$\Rightarrow r^2\frac{dV_r}{dr} = \left(\frac{3i}{2C_1}\right)^{\frac{2}{3}}\left(r + C_2\right)^{\frac{2}{3}}$$

$$\frac{dV_r}{dr} = \left(\frac{3i}{2C_1}\right)^{\frac{2}{3}}\frac{1}{r^2}\left(r + C_2\right)^{\frac{2}{3}}\ .$$

This is the expression for the corrected radial electric field.

Appendix C

Table of Data of the graphs in Chapter 7

Table A.1: calculated parameters of the thruster

Current (A)	Voltage ($V - V_0$) (V)	Vector heating Thrust (N)	Electrostatic Thrust (N)
0.000005	209.123	3.14E-06	1.08E-05
0.00001	376.197	6.53E-06	3.39E-05
0.000015	526.4247	1.01E-05	6.17E-05
0.00002	665.8917	1.39E-05	9.13E-05
0.000025	797.5077	1.78E-05	0.000121
0.00003	922.9828	2.18E-05	0.000152
0.000035	1043.441	2.6E-05	0.000182
0.00004	1159.677	3.02E-05	0.000212
0.000045	1272.278	3.46E-05	0.000241
0.00005	1381.7	3.91E-05	0.000271
0.000055	1488.301	4.37E-05	0.0003
0.00006	1592.373	4.83E-05	0.000329
0.000065	1694.157	5.31E-05	0.000358
0.00007	1793.856	5.79E-05	0.000386

Where the above table values are calculated for:

The voltage according to equation (4.19)

$$V-V_0=\left[\frac{-(D+C_2)^{\frac{2}{3}}}{D}+\frac{1}{3b}\ln\left[\frac{\frac{(D+C_2)^{\frac{2}{3}}}{b^2}-\frac{2(D+C_2)^{\frac{1}{3}}}{b}+1}{\frac{(D+C_2)^{\frac{2}{3}}}{b^2}+\frac{(D+C_2)^{\frac{1}{3}}}{b}+1}\right]+\frac{\sqrt{12}}{3b}\arctan\left[\frac{2}{\sqrt{3}}\frac{(D+C_2)^{\frac{1}{3}}}{b}+\frac{1}{\sqrt{3}}\right]\right.$$

$$\left.-\frac{1}{3b}\ln\left[\frac{\frac{(R+C_2)^{\frac{2}{3}}}{b^2}-\frac{2(R+C_2)^{\frac{1}{3}}}{b}+1}{\frac{(R+C_2)^{\frac{2}{3}}}{b^2}+\frac{(R+C_2)^{\frac{1}{3}}}{b}+1}\right]-\frac{\sqrt{12}}{3b}\arctan\left[\frac{2}{\sqrt{3}}\frac{(R+C_2)^{\frac{1}{3}}}{b}+\frac{1}{\sqrt{3}}\right]\right]\cdot\left(\frac{3i}{2C_1}\right)^{\frac{2}{3}},$$

The "Vector heating" thrust according to equation (5.7)

$$F=\dot{m}\sqrt{\frac{3K}{M}}\left[\left(\frac{P-I'}{\dot{m}C}+T_1\right)^{1/2}-T_1^{1/2}\right],$$

And the electrostatic thrust according to equation (5.10)

$$F_T=\frac{i}{C_0}\cdot\left(\frac{3i}{2C_1}\right)^{\frac{1}{3}}\left[\frac{-(D+C_2)^{\frac{1}{3}}}{D}+\frac{1}{6b^2}\ln\left[\frac{\frac{(D+C_2)^{\frac{2}{3}}}{b^2}-\frac{2(D+C_2)^{\frac{1}{3}}}{b}+1}{\frac{(D+C_2)^{\frac{2}{3}}}{b^2}+\frac{(D+C_2)^{\frac{1}{3}}}{b}+1}\right]+\frac{\sqrt{12}}{6b^2}\arctan\left[\frac{2}{\sqrt{3}}\frac{(D+C_2)^{\frac{1}{3}}}{b}+\frac{1}{\sqrt{3}}\right]\right]$$

$$-\frac{i}{C_0}\cdot\left(\frac{3i}{2C_1}\right)^{\frac{1}{3}}\left[\frac{-(R+C_2)^{\frac{1}{3}}}{R}+\frac{1}{6b^2}\ln\left[\frac{\frac{(R+C_2)^{\frac{2}{3}}}{b^2}-\frac{2(R+C_2)^{\frac{1}{3}}}{b}+1}{\frac{(R+C_2)^{\frac{2}{3}}}{b^2}+\frac{(R+C_2)^{\frac{1}{3}}}{b}+1}\right]+\frac{\sqrt{12}}{6b^2}\arctan\left[\frac{2}{\sqrt{3}}\frac{(R+C_2)^{\frac{1}{3}}}{b}+\frac{1}{\sqrt{3}}\right]\right].$$

References

[1] George P. Sutton, Oscar Biblarz, *Rocket Propulsion Elements,* Seventh Edition, John Wiley& Sons, New York, 2001.

[2] Peter Fortescue, John Stark, Graham Swinerd, *Spacecraft Systems Engineering*, Third Edition, John Wiley& Sons Ltd, England, 2003.

[3] Stuhlinger E., *Ion Propulsion for Space Flight*, McGraw-Hill, New York, 1964.

[4] John R. Brophy, *NASA's deep space 1 Ion Engine,* ICIS-01-20.1, 2000.

[5] Joseph F. Masi, Howard Seifert, *Advanced Propulsion Concepts,* Gordon and Breach Science Publishers, 1966.

[6] Jahn R. G., Choueiri E. Y., *Electric Propulsion,* Encyclopedia of Physical Science and Technology, Third edition, Volume 3, 2002.

[7] A. Theodore Forrester, Guntis Kuskevics, *Ion Propulsion*, AIAA 1969

[8]Maxwell W. Hunter, II, *Thrust Into Space*, Holt, Rinehart and Winston, INC, United States of America, 1966

[9] Manuel Martinez-Sanchez *Lecture 13-14: Electrostatic Thrusters*, 16.522 Space Propulsion course lecture notes, Massachusetts Institute of Technology

[10] The internet Encyclopedia of Science: *Advanced Propulsion Concepts,* Available: http://WWW.daviddarling.info/encyclopedia/A/advanced_propulsion_concepts.html [February 10, 2011]

[11] "Matter, States of", Microsoft® Encarta® 2009 [DVD]. Microsoft Corporation, 2008

[12] F. Llewellyn-Jones, *Ionization and breakdown in gases*, Methuen& Co LTD London, 1966

[13] Hill Philip G., *Mechanics and thermodynamics of propulsion,* Addison Wesley Publishing Company, Inc, 1992.

[14] Heister, Stephen. *"Rocket."* World Book Online Reference Center. 2005. Available: http://www.worldbookonline.com [February 10, 2011]

[15] N. H. Langton, *Rocket Propulsion*, University of London Press Ltd, 1970.

[16] 'University of Michigan Plasmadynamics and Electric Propulsion Laboratory Thrusters'.2002. Available:

http://aerospace.engin.umich.edu/spacelab/thrusters/thrusters.html.

[February 10, 2011]

[17] 'Electrostatic Ion Thruster'. 2009. Available:

http://en.wikipedia.org/wiki/Electrostatic_ion_thruster. [February 10, 2011]

[18] T. Lafleur, *Corona discharge as an ionization mechanism for electrostatic propulsion applications*, Honors project Wits University, 2007.

[19] 'NSTAR Ion Engine'. 1999. Available:

http://www.boeing.com/defensespace/space/bss/factsheets/xips/nstar/ionengine.html. [February 10, 2011]

[20] Essam Nasser, *Fundamentals of gaseous ionization and plasma electronics*, John Wiley & Sons New York, 1971

[21] E. Kuffel, W.S. Zaengl, J. Kuffel, *High Voltage Engineering: Fundamentals*, E. Kuffel, W.S. Zaengl, J. Kuffel, Amsterdam, 2000.

[22] H. Raether, *Electron Avalanches and Breakdown in Gases*, Butter Worths London, 1964

[23] Loeb L., *Electrical Coronas: Their Basic Physical Mechanisms*, University of California Press, Berkley and Los Angeles, 1965.

[24] Peek. F. W., *Dielectric Phenomena in High Voltage Engineering.* McGraw Hill [48-108], 1929.

[25] Adiv Maimon, *Investigation of Corona ionization Electric Engine for Spacecraft Propulsion*, Final Thesis Report, University of Cape Town, 2009

[26] 'Ionization'. 2009. Available: http://en.wikipedia.org/wiki/Ionization. [February 10, 2011]

[27] J. S. Townsend, *The Potentials required to Maintain Currents between Coaxial Cylinders*, The Philosophical magazine 36 pages 83-90, 1945.

[28] J. W. Luginsland, Y. Y. Lau, and R. M. Gilgenbach, *Two-Dimensional Child-Langmuir Law*, Physical Review Letters, Volume 77, Number 22, 25 November 1996

[29] M. Goldman, A. Goldman and R. S. Sigmond, *The Corona discharge, its Properties and Specific Uses*, Pure & Appi. Chem., Vol. 57, No. 9, pp. 1353—1362, 1985

[30] Jack Wilson, Hugh D. Perkins and William K. Thompson, *An Investigation of Ionic Wind Propulsion*, NASA/TM—2009-215822